

How slab age and width combine to dictate the dynamics and evolution of subduction systems: a 3-D spherical study

Fangqin Chen¹, D. Rhodri Davies¹, Saskia Goes², Lior Suchoy², and Stephan C Kramer²

¹Australian National University

²Imperial College London

November 24, 2022

Abstract

Many of the factors expected to control the dynamics and evolution of Earth's subduction zones are under-explored in an Earth-like spherical geometry. Here, we simulate multi-material free-subduction of a complex rheology slab in a 3-D spherical shell domain, to investigate the effect of plate age (simulated by covarying plate thickness and density) and width on the evolution of subduction systems. We find that the first-order predictions of our spherical cases are generally consistent with existing Cartesian studies: (i) as subducting plate age increases, slabs retreat more and subduct at a shallower dip angle, due to increased bending resistance and sinking rates; and (ii) wider slabs can develop along-strike variations in trench curvature due to toroidal flow at slab edges, trending towards a 'W'-shaped trench with increasing slab width. We find, however, that these along-strike variations are restricted to older, stronger, retreating slabs. Younger slabs that drive minimal trench motion remain relatively straight along the length of the subduction zone. We summarise our results into a regime diagram, which highlights how slab age modulates the effect of slab width, and present examples of the evolutionary history of subduction zones that are consistent with our model predictions.

1 **How slab age and width combine to dictate the**
2 **dynamics and evolution of subduction systems:**
3 **a 3-D spherical study**

4 **Fangqin Chen¹, D. Rhodri Davies¹, Saskia Goes²,**
5 **Lior Suchoy², Stephan C. Kramer²**

6 ¹Research School of Earth Sciences, The Australian National University, Canberra, ACT, Australia
7 ²Department of Earth Science and Engineering, Imperial College London, London, UK

8 **Key Points:**

- 9 • Spherical models are used to examine the joint effect of slab age and width on free
10 subduction dynamics.
11 • Older slabs enhance trench retreat whilst wider slabs can drive along-strike vari-
12 ations in shape.
13 • The effect of plate width is strongly modulated by plate age, given its control on
14 trench retreat.

Corresponding author: Fangqin Chen, Fangqin.Chen@anu.edu.au

Abstract

Many of the factors expected to control the dynamics and evolution of Earth’s subduction zones are under-explored in an Earth-like spherical geometry. Here, we simulate multi-material free-subduction of a complex rheology slab in a 3-D spherical shell domain, to investigate the effect of plate age (simulated by covarying plate thickness and density) and width on the evolution of subduction systems. We find that the first-order predictions of our spherical cases are generally consistent with existing Cartesian studies: (i) as subducting plate age increases, slabs retreat more and subduct at a shallower dip angle, due to increased bending resistance and sinking rates; and (ii) wider slabs can develop along-strike variations in trench curvature due to toroidal flow at slab edges, trending towards a ‘W’-shaped trench with increasing slab width. We find, however, that these along-strike variations are restricted to older, stronger, retreating slabs. Younger slabs that drive minimal trench motion remain relatively straight along the length of the subduction zone. We summarise our results into a regime diagram, which highlights how slab age modulates the effect of slab width, and present examples of the evolutionary history of subduction zones that are consistent with our model predictions.

Plain Language Summary

Subduction zones are locations where Earth’s tectonic plates collide, and the denser plate subsequently descends into the mantle. They exert important controls on surface plate motions, plate boundary deformation, mountain-building, seismic hazard, volcanism, and help to organise underlying mantle flow, which is the engine driving our dynamic Earth. As a result, this important process has been extensively studied through both analogue and computational models. Here, we model the dynamics and evolution of subduction systems on an Earth-like sphere, and find that: (i) older plates, which have spent longer cooling at Earth’s surface, sink into the underlying mantle faster, at a shallower angle; and (ii) narrower plates tend to develop ‘C’-shaped trenches, whereas wider plates tend to develop ‘W’-shaped trenches. Importantly, the influence of subducting plate width is strongly dependent on its age. We show how these two factors combined can explain key aspects of the evolution of several major subduction zones on Earth.

1 Introduction

During subduction, the oceanic lithosphere of one tectonic plate dives beneath another at a convergent margin and is recycled into Earth’s mantle (e.g., Stern, 2002; Kearey et al., 2009). As subducted slabs descend, their negative buoyancy provides a key driving force for plate tectonics, and they continue to influence surface processes in a number of ways (e.g., Forsyth & Uyeda, 1975; Mitrovica et al., 1989; Lithgow-Bertelloni & Richards, 1998; Wheeler & White, 2002; Perrin et al., 2018; Rubey et al., 2017; Beall et al., 2021). Seismic images of Earth’s interior reveal that when slabs descend towards the mantle transition zone, at depths of 410–660 km that coincide with several mineralogical phase transformations and a likely viscosity increase (e.g., Hager & Richards, 1989), some stall and are horizontally deflected (e.g., the Ryuku, Izu-Bonin and Honshu slabs), some thicken and buckle (e.g., the Marianas slab), whilst others appear to pass through unhindered (e.g., the Cocos and Antilles slabs). Their imaged morphologies are therefore far from uniform (e.g., Karato et al., 2001; Li et al., 2008; Fukao & Obayashi, 2013a; Goes et al., 2017; van der Meer et al., 2018). The dominant controls on such variations remain unclear, and likely vary between different subduction zones, due to complexities arising from non-linear and multi-scale interactions between several aspects of the mantle system, including downgoing and overriding plate properties, global mantle flow, mineral phase changes and material rheology (e.g., Karato et al., 2001; Čížková et al., 2002; Capitanio et al., 2007; Schellart et al., 2007; Goes et al., 2008; Stegman, Farrington, et

64 al., 2010; Garel et al., 2014; Goes et al., 2017; Agrusta et al., 2017; Alsaif et al., 2020;
65 Holt & Royden, 2020; Garel et al., 2020; Suchoy et al., 2021).

66 The observational record does not support a clear correlation between slab mor-
67 phology and subducting plate age (e.g., Lallemand et al., 2005; Sdrolias & Müller, 2006;
68 Goes et al., 2011). This implies that other factors strongly influence the evolution of sub-
69 duction systems, including variations in a slab’s age along the trench, trench width, lo-
70 cal sources of buoyancy such as oceanic plateaus and aseismic ridges, regional tecton-
71 ics, and complexities associated with overriding plates. Several studies have investigated
72 how these aspects control the evolution of subducted slabs, mostly in either 2-D or 3-
73 D Cartesian domains, in an attempt to reconcile predictions from geodynamical mod-
74 elling with the observed morphologies (e.g., Morra et al., 2006; Čížková et al., 2007; Schel-
75 lart et al., 2007; Capitanio et al., 2010; Martinod et al., 2010; Mason et al., 2010; Stegman,
76 Farrington, et al., 2010; Rodríguez-González et al., 2012; Sharples et al., 2014; Garel et
77 al., 2014; Čížková & Bina, 2015; Holt et al., 2018).

78 The age of a subducting slab determines its thermal structure, which controls slab
79 thickness, density and rheology. In turn, these control slab buoyancy and strength, which
80 combine to determine the rate of trench retreat (e.g., Bellahsen et al., 2005; Capitanio
81 et al., 2007; Di Giuseppe et al., 2008; Schellart, 2008; Ribe, 2010; Stegman, Farrington,
82 et al., 2010; Garel et al., 2014; Goes et al., 2017). It is well-established that trench-motion
83 history correlates with slab morphology (e.g., van der Hilst & Seno, 1993; Faccenna et
84 al., 2001; Goes et al., 2017). Goes et al. (2008) suggest that older, colder, oceanic litho-
85 sphere is stronger due to the temperature dependence of viscosity, and that this drives
86 significant trench retreat, with slabs more likely to lie flat at the mantle transition zone;
87 conversely, younger lithosphere is weaker and subducts with less trench retreat, tend-
88 ing to buckle at the mantle transition zone. This direct link between slab age and the
89 style of slab-transition zone interaction is supported by laboratory and numerical sim-
90 ulations (e.g., Schellart, 2004; Bellahsen et al., 2005; Capitanio et al., 2007; Funicello
91 et al., 2008; Garel et al., 2014; Goes et al., 2017).

92 Slab width also plays an important role in determining the evolution of subduc-
93 tion zones, affecting the shape and curvature of the trench, by influencing the rate of trench
94 retreat (e.g., Bellahsen et al., 2005; Stegman et al., 2006; Schellart et al., 2007; Stegman,
95 Schellart, & Freeman, 2010; Strak & Schellart, 2016). Schellart et al. (2007) advocate
96 an inversely proportional relationship between trench migration rates and the width of
97 subduction zones. In their models, wider slabs develop upper mantle stagnation zones,
98 where the centre of the trench exhibits negligible trench retreat relative to its edges. Such
99 a relationship is observed in large subduction systems such as the South American sub-
100 duction zone, and could be responsible for the varying styles of slab morphology observed
101 along wide trenches.

102 Plate interactions and lateral variations in plate properties also influence the ge-
103 ometry and evolution of subducting slabs. The structure and motion of overriding plates
104 have an effect on slab dip, trench migration, and slab interaction with the mantle tran-
105 sition zone (e.g., Jarrard, 1986; Lallemand et al., 2005; Heuret et al., 2007; Capitanio
106 et al., 2010; van Dinther et al., 2010; Garel et al., 2014). Interactions with nearby past
107 or ongoing subduction zones may also affect the sinking velocity and slab penetration
108 of the mantle transition zone (e.g., Fukao et al., 2009; Becker & Faccenna, 2011; Fukao
109 & Obayashi, 2013b; Čížková & Bina, 2019). The subduction of locally thickened oceanic
110 lithosphere, such as oceanic plateaus, aseismic ridges or seamount chains, has been pro-
111 posed to influence the shape of the trench and change the geometry of subducting slabs
112 (e.g., Cross & Pilger, 1982; Gutscher, Malavieille, et al., 1999; Martinod et al., 2005; Cap-
113 itanio et al., 2011; Suchoy et al., 2022). The higher compositional buoyancy of oceanic
114 plateaus and ridges could resist slab sinking into the mantle and, thus, potentially lead
115 to flat slab subduction (e.g., van Hunen et al., 2002; Mason et al., 2010). These factors

116 add to the complexity of observed slab morphology, and may explain why no simple cor-
 117 relations can be made with plate properties.

118 Existing numerical and laboratory studies in an enclosed Cartesian domain pro-
 119 vide valuable insight into the sensitivity of slab morphology to a number of these con-
 120 trolling parameters. However, such models neglect the role of Earth’s sphericity, the ge-
 121 ometric consequences of which results in curved subduction zones, the build-up of lat-
 122 eral strain, buckling along the trench, and an increase in the geometric stiffness of slabs
 123 (e.g., Frank, 1968; Laravie, 1975; Bayly, 1982; Fukao et al., 1987; Yamaoka, 1988; Tan-
 124 imoto, 1998; Mahadevan et al., 2010; Schettino & Tassi, 2012).

125 In this paper, our aim is to investigate the effect of subducting plate age and width
 126 on slab morphology using 3-D spherical shell numerical models of free subduction. Only
 127 a limited number of spherical subduction models have investigated the dynamics of sub-
 128 duction, and these considered only isoviscous plates (e.g. Morra et al., 2009, 2012; But-
 129 terworth et al., 2012, 2014; Chamolly & Ribe, 2021). To more realistically approximate
 130 subduction on Earth, especially for wider plates, we will present the first multi-material
 131 subduction models with a composite plate rheology in a spherical shell domain. We con-
 132 sider plate ages (estimated with three combinations of plate thickness and density) rang-
 133 ing from young (~ 10 Myr, estimated using a half space cooling model) to old (~ 140 Myr),

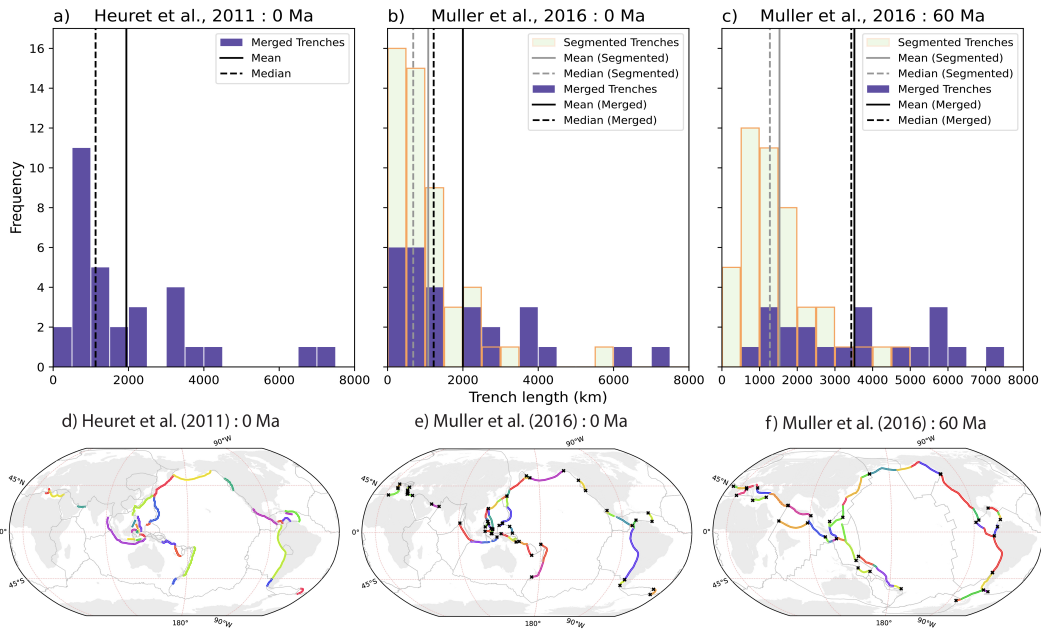


Figure 1. (a) Present-day trench length histogram compiled from rupture segment lengths by Heuret et al. (2011) and combined here for commonly recognised continuous trenches; (b) and (c) trench length histograms based on global tectonic plate reconstructions, at the present day and at 60 Ma, respectively Müller et al. (2016). The reconstructed trenches are segmented based on changes in lower or upper plate characteristics (green bars with orange outline). Based on lower plate properties, we merged segments that likely subduct as coherent slabs (purple bars). (d) Map of subduction zones from Heuret et al. (2011). (e) and (f) Map of trench segments based on plate reconstruction at present and at 60 Ma by Müller et al. (2016). In (e) and (f), black crosses represent edges of subduction zones. Trench segments within each subduction zone were merged when calculating trench length.

134 noting that the range of subducting plate ages on Earth at present day is 0 - 160 Myr
 135 (e.g. Müller et al., 2016). Motivated by a compilation of global trench lengths at the present
 136 day (Heuret et al., 2011) and Cenozoic Era reconstructions (Müller et al., 2016), we ex-
 137 amine trench widths of 1200, 2400, 3600 and 4800 km. As illustrated in Figure 1, at the
 138 present day, most trenches are less than 5000 km wide, with mean and median widths
 139 of 1940 km and 1130 km for the dataset of Heuret et al. (2011) and 2000 km and 1230 km
 140 for the dataset of Müller et al. (2016). At 60 Ma (where there are less data on narrow
 141 trenches), mean and median widths are 3520 km and 3430 km (Müller et al., 2016). It
 142 is noteworthy that very few trenches exceed 6000 km in width: at present, the South Amer-
 143 ica trench is 7060 km wide, and the Andaman-Sumatra-Java-Timor trench exceeds 6040 km
 144 width; at 60 Myr, the South America and Aleutian trenches were ~ 7100 and ~ 6070 km
 145 wide, respectively (Müller et al., 2016).

146 In this paper, we present, for a systematic set of simulations, a quantitative com-
 147 parison to demonstrate how slab thickness and density (approximating the buoyancy of
 148 slabs of different age) and slab width affects the evolution of subducting slabs. We then
 149 discuss the likely mechanisms that can explain our results and their implications for an
 150 improved understanding of subduction on Earth.

151 2 Model Description

152 2.1 Governing Equations and Numerical Strategy

153 We simulate multi-material free-subduction of a composite visco-plastic plate into
 154 an ambient mantle, in a 3-D hemispherical shell domain, which extends from the sur-
 155 face to the core-mantle-boundary (CMB) at a depth of 2890 km. Assuming incompress-
 156 ibility, the governing equations for this problem are the continuity equation,

$$157 \quad \nabla \cdot \mathbf{u} = 0 \quad (1)$$

158 the conservation of momentum equation for infinite Prandtl number,

$$159 \quad -\vec{\nabla} p + \nabla \cdot \left[\mu \left(\vec{\nabla} \mathbf{u} + \left(\vec{\nabla} \mathbf{u} \right)^T \right) \right] = g \Delta \rho \Gamma \hat{k} \quad (2)$$

160 and an advection equation for composition,

$$161 \quad \frac{\partial \Gamma}{\partial t} + \mathbf{u} \cdot \vec{\nabla} \Gamma = 0 \quad (3)$$

162 where \mathbf{u} is velocity, p the pressure, μ the viscosity, ρ the density, g gravity acceleration,
 163 \hat{k} unit vector in the direction opposite gravity, and Γ the material volume fraction ($\Gamma =$
 164 1 in a region occupied by a given material and $\Gamma = 0$ elsewhere).

165 Simulations are carried out using Fluidity (e.g., Davies et al., 2011; Kramer et al.,
 166 2012; Davies et al., 2016), an anisotropic, adaptive, unstructured mesh computational
 167 modelling framework supporting finite element and control volume discretisations. Flu-
 168 idity has recently been validated for simulations in a spherical shell domain against an
 169 extensive set of analytical solutions introduced by Kramer et al. (2021). It has also been
 170 validated for visco-plastic simulations like those examined herein (e.g. Le Voci et al., 2014;
 171 Tosi et al., 2015). In the context of this study, Fluidity has several favourable features.
 172 The framework: (i) uses an unstructured mesh, which enables the straightforward rep-
 173 resentation of complex geometries and materials; (ii) dynamically optimizes this mesh,
 174 across parallel processors, providing increased resolution in areas of dynamic importance,
 175 thus allowing for accurate simulations across a range of length-scales, within a single model;
 176 (iii) enhances mesh optimization using anisotropic elements; (iv) can employ a free-surface
 177 boundary condition, which is important for correctly capturing slab decoupling from the
 178 surface (Kramer et al., 2012); (v) utilises the highly-scalable parallel linear system solvers
 179 available in PETSc (Balay et al., 1997, 2021a, 2021b), which can efficiently handle sharp,

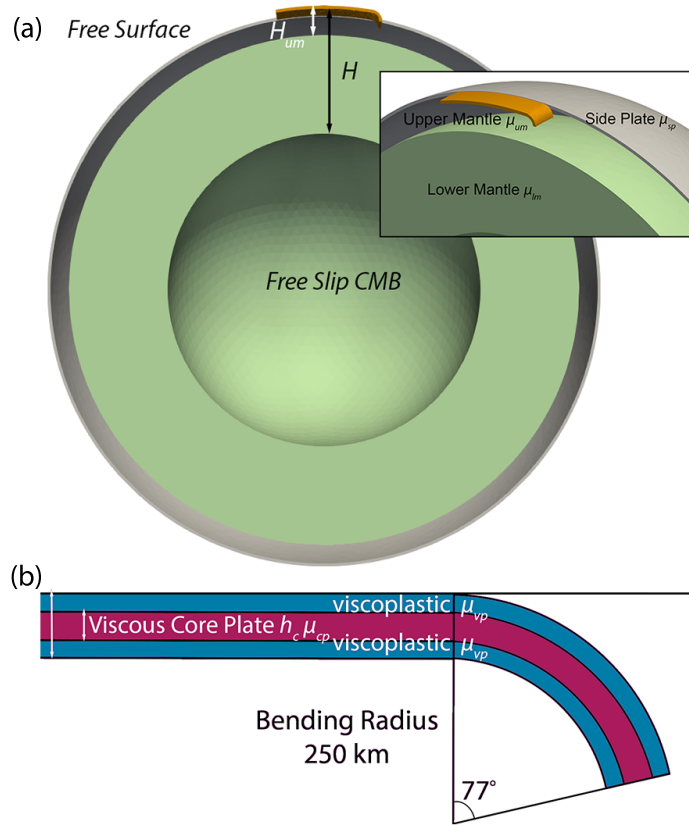


Figure 2. (a) Setup of our simulations in a spherical geometry. We exploit the symmetry of the system, allowing us to halve the computational domain’s extent, whilst inner and outer boundaries approximate Earth’s core-mantle-boundary and surface, respectively. (b) Initial slab tip geometry of our layered visco-plastic plates.

180 orders of magnitude variations in viscosity; and (vi) has a novel interface-preservation
 181 scheme, which conserves material volume fractions and allows for the incorporation of
 182 distinct materials (Wilson, 2009). In this study, Fluidity’s adaptive mesh capabilities are
 183 utilised to provide a local resolution of 3 km in regions of dynamic significance (i.e. at
 184 the interface between materials and in regions of strong velocity and viscosity contrasts),
 185 with a coarser resolution of up to 300 km elsewhere. It is this adaptive mesh function-
 186 ality that makes our spherical shell simulations computationally tractable.

187 2.2 Geometry, Boundary Conditions and Material Properties

188 The configuration of our models is inspired by Stegman, Farrington, et al. (2010)
 189 and Garel et al. (2014). Simulations exploit the symmetry of the system to halve the com-
 190 putational domain’s extent, modelling half of the plate width in a hemispherical shell.
 191 When non-dimensionalised, the hemispherical shell has an outer radius of 2.22 and an
 192 inner radius 1.22, thus the computational domain has a thickness of 1. Models have a
 193 free-surface boundary condition on the outer surface, and a free-slip condition on the sym-
 194 metry plane and CMB, as illustrated in Figure 2 (a). Gravity acts radially, towards the
 195 centre of the sphere.

Table 1. Parameters common to all simulations.

Parameter	Symbol	Value
Gravitational acceleration	g	10 m/s ²
Characteristic depth (whole mantle)	H	2890 km
Depth of upper mantle	H_{um}	660 km
Upper mantle reference viscosity	μ_{um}	2.0×10^{20} Pa s
Lower mantle reference viscosity	μ_{lm}	$50 \times \mu_{um}$
Core plate viscosity	μ_{cp}	$100 \times \mu_{um}$
Initial viscosity of visco-plastic layer	μ_{Newt}	$100 \times \mu_{um}$
Side plate viscosity	μ_{sp}	$1000 \times \mu_{um}$
Mantle density	ρ	3300 kg/m ³
Yield stress	τ_{yield}	100 MPa

The subducting plate length (L) is 2200 km. The initial slab tip geometry is prescribed with a bending radius of 250 km and an angle of 77°, resulting in a 336 km-long slab tip (Figure 2b). The subducting lithosphere comprises a composite plate of constant initial thickness with a core isoviscous layer embedded in upper and lower visco-plastic layers with viscosities that follow a von Mises law. Upper and lower visco-plastic layers are used to approximate the strain-rate weakening that occurs above and below the slab core in thermo-mechanical simulations of subduction (e.g. Garel et al., 2014), following OzBench et al. (2008). Upper and lower layers are assigned the minimum viscosity between the Newtonian viscosity μ_{Newt} and an effective von Mises viscosity μ_{vM} , such that purely viscous deformation occurs as long as the second invariant of the stress tensor $\tau_{II} = 2\mu\dot{\epsilon}_{II}$ (where $\dot{\epsilon}_{II}$ is the second invariant of strain rate tensor) does not reach the critical yield stress, τ_{yield} . The effective viscosity of the visco-plastic layers is given by:

$$\mu_{vM} = \begin{cases} \frac{\tau_{II}}{2\dot{\epsilon}_{II}}, & \text{if } \tau < \tau_{yield} \\ \frac{\tau_{yield}}{2\dot{\epsilon}_{II}}, & \text{if } \tau \geq \tau_{yield} \end{cases} \quad (4)$$

At material interfaces, the average viscosity is calculated through a geometric mean,

$$\mu_{ave} = \mu_1^{\Gamma_1} \mu_2^{\Gamma_2}, \quad (5)$$

196 where μ_i is the viscosity of material i , and Γ_i is the relative volume fraction of material
197 i in the vicinity of the finite-element node at which the effective viscosity μ_{ave} is needed.

198 The subducting plate is surrounded by mantle material, with no overriding or trailing
199 plate. When the plate advances, the mantle material fills in behind the trailing edge.
200 A dome-shaped side plate covers the entire domain adjacent to the subducting plate. It
201 has the same thickness as the subducting plate, and is placed 22 km away from the plate's
202 edge, keeping a constant distance from the symmetry plane around the base of the dome.
203 The side plate is 1000 times more viscous than adjacent upper mantle material, and pre-
204 vents lateral flow from narrowing the width of downgoing plate (as in Holt et al., 2017).
205 The lower mantle below 660 km depth is 50 times more viscous than the upper mantle.
206 The viscosity jump is a simplified parameterisation of the transition zone's hindering ef-
207 fect of the mantle flow from upper mantle into lower mantle, from not only the viscos-
208 ity increase with depth but also the endothermic phase transition that is excluded from
209 the model, as in Stegman, Farrington, et al. (2010). Model parameters common to all
210 simulations are listed in Table 1.

Table 2. Simulations examined and associated model parameters.

Case	h (km)	h_c (km)	$\Delta\rho$ (kg m ⁻³)	w (km)
W1200_young	45	15	40	1200
W1200_ref	70	30	80	1200
W1200_old	100	40	120	1200
W2400_young	45	15	40	2400
W2400_ref	70	30	80	2400
W2400_old	100	40	120	2400
W3600_young	45	15	40	3600
W3600_ref	70	30	80	3600
W3600_old	100	40	120	3600
W4800_young	45	15	40	4800
W4800_ref	70	30	80	4800
W4800_old	100	40	120	4800

2.3 Cases Examined and Quantitative Model Diagnostics

We investigate 12 cases across a wide parameter-space. We systematically varied plate width (w) and plate 'age', represented by co-varying plate thickness (h), core thickness (h_c), and density contrast between the plate and adjacent mantle ($\Delta\rho$) to capture the joint increase of negative plate buoyancy and bending strength with age. This allows us to examine how these two factors influence the evolution of subduction and slab morphologies. Our choices are motivated by subduction regime diagrams, as a function of plate age or plate width, from other studies (e.g., Stegman, Schellart, & Freeman, 2010; Garel et al., 2014; Goes et al., 2017). The selected combinations of plate thickness and density contrast produce diverse subduction behaviours, ranging from a vertical-folding type young plate to a retreating and flattening old plate. We note that in the following sections, specified plate widths refer to the full width of the plate (i.e. twice the width simulated, owing to the symmetry plane). Case names, alongside their key parameter values, are listed in Table 2.

To quantify the sensitivity of results to these parameters, we have calculated several diagnostic outputs. When doing so, the boundary of the slab is defined as the 0.5 contour of the mantle material volume fraction (material volume fraction = 1 when the material is mantle, 0 otherwise). Based on this contour, we extract the slab tip depth, the trench location (measured at 15 km depth), and the trailing edge position, as well as rates of slab descent, trench retreat and plate advance. We extract the fastest vertical sinking velocity at the symmetry plane; as well as the maximum sinking velocity throughout the entire domain. We calculate the average slab dip in the upper mantle from the surface to 650 km depth, with respect to the direction of gravity at the slab centre at 325 km depth, which is radially towards the centre of the sphere from the point of measurement. Measurements are taken at the symmetry plane unless otherwise specified. We also trace the evolution of trench geometry relative to the initial trench shape.

3 Results

3.1 Reference Case

Case W1200_ref is selected as our reference, given its mid-range plate buoyancy and thickness (McKenzie et al., 2005), and width that sits towards the lower end of trench lengths on Earth. The temporal evolution of this case is illustrated in Figure 3(a). As subduction starts, the slab tip steepens. During the upper mantle sinking phase (Fig-

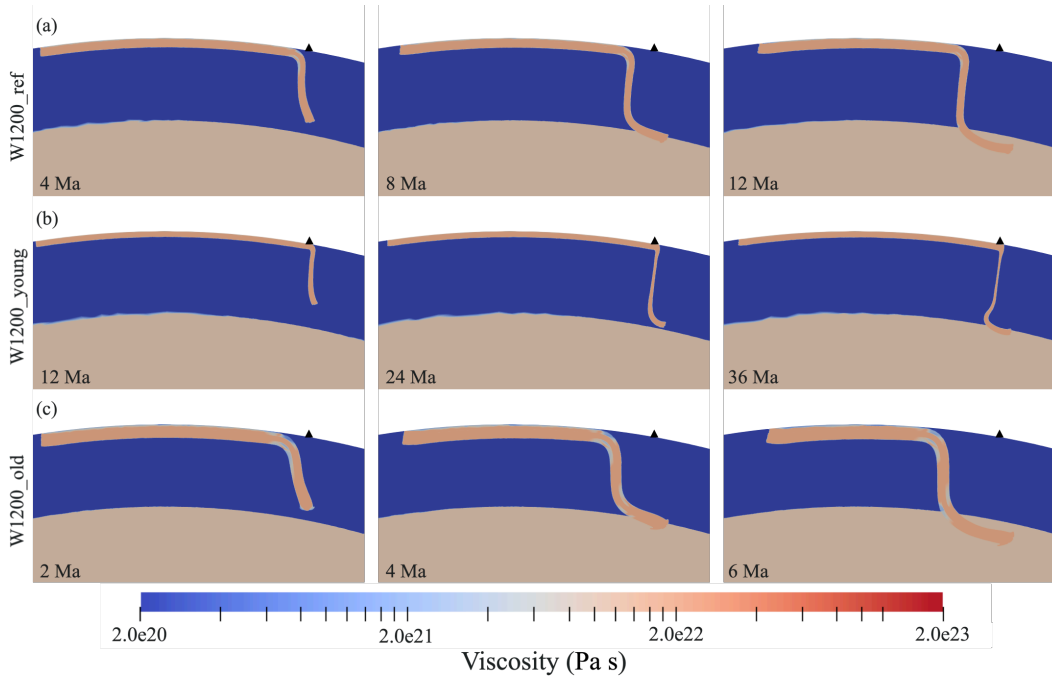


Figure 3. Snapshots illustrating the spatio-temporal evolution of slab morphology as reflected in the viscosity field, for models with a plate width of 1200 km: (a) W1200_ref, with $H = 70$ km and $\Delta\rho = 80 \text{ kg m}^{-3}$; (b) W1200_young, with $H = 45$ km and $\Delta\rho = 40 \text{ kg m}^{-3}$; (c) W1200_old, with $H = 100$ km and $\Delta\rho = 120 \text{ kg m}^{-3}$.

243 ure 4a), the trench steadily retreats from its initial position (Figure 4b) with $\sim 50\%$ of
 244 subduction accommodated via this trench retreat (over 60% in the early stages), despite
 245 the trailing edge of the plate advancing steadily (Figure 4c,d). As the trench retreats,
 246 it develops a concave ‘C’ shape, as illustrated in Figure 5(b). Following interaction with
 247 the viscosity jump at 660 km depth, the slab tip is deflected, the slab sinking rate reduces
 248 substantially (Figure 4a,e), and the upper mantle section of the slab steepens (Figure
 249 4f). The slab then slowly sinks into the lower mantle.

250 Coupling between the sinking plate and the adjacent mantle drives toroidal and
 251 poloidal mantle flow (e.g., Schellart, 2004; Funiciello et al., 2006; Stegman et al., 2006).
 252 Figure 6(a-c) illustrates horizontal flow at 300 km depth at different stages of subduc-
 253 tion: trench/slab retreat drives toroidal flow around the edge of the plate, which pro-
 254 motes increased trench concavity (Figure 5b). Figure 6(d-f) shows vertical cross-sections
 255 through the symmetry plane: two poloidal cells can be identified as the slab sinks in the
 256 upper mantle, one above the downgoing plate in the mantle wedge, and the other in the
 257 sub-slab region. During the upper-mantle phase of subduction, the mantle wedge cell
 258 is more prominent, while flow velocities in this cell diminish as the slab tip deflects and
 259 sinks into the more viscous lower mantle.

260 3.2 Influence of subducting plate age

261 The two cases, W1200_young and W1200_old, were designed to demonstrate how
 262 plate age (through its joint effect on buoyancy and strength) modifies subduction dy-
 263 namics. Our parameter values approximate the properties of younger (decreased $\Delta\rho$ and
 264 H) and older (increased $\Delta\rho$ and H) plates, respectively.

265 The younger slab (W1200_young) stretches and sinks almost vertically through the
 266 upper mantle as it subducts, folding upon interaction with the upper-lower mantle in-
 267 terface (Figures 3b and 4e). Trench location remains almost fixed (Figure 4b) and trench
 268 shape does not evolve much over time (Figure 5a). Excluding the initial phase of sub-
 269 duction, trench retreat is minimal: within 5 Myr of the start of subduction, $\sim 80\%$ of
 270 subduction is accommodated by plate advance (Figure 4d).

271 The older case (W1200_old) exhibits the fastest sinking, trench retreat and plate
 272 advance velocities among all cases examined at this width (Figure 4). The slab tip sinks
 273 in the upper mantle at a shallower angle than the younger cases (Figure 4f). It is de-
 274 flected at the mantle transition zone, and the sinking rate decreases as the slab moves
 275 into the lower mantle (Figure 4a,e). Similar to the reference case, after reaching 660 km
 276 depth, the upper mantle portion of the slab gradually steepens (Figure 3c). Trench re-
 277 treat is substantial and accommodates much of the subduction (the trench retreat to to-
 278 tal descent ratio remains above $\sim 55\%$ throughout the simulation – Figure 4b,d), with
 279 the trench developing a concave curvature over time (Figure 5c).

280 The cases examined at 1200 km width clearly display a range of behaviours, with
 281 a strong sensitivity to the age, i.e. buoyancy and strength, of the subducting slab. The
 282 younger plate exhibits the weakest behaviour, manifested by a steeper upper mantle sub-
 283 duction angle and minimal trench retreat, with subduction principally accommodated
 284 via plate advance. This case falls into the vertical folding regime (e.g., Schellart, 2008;
 285 Stegman, Farrington, et al., 2010; Garel et al., 2014; Goes et al., 2017). The older plate

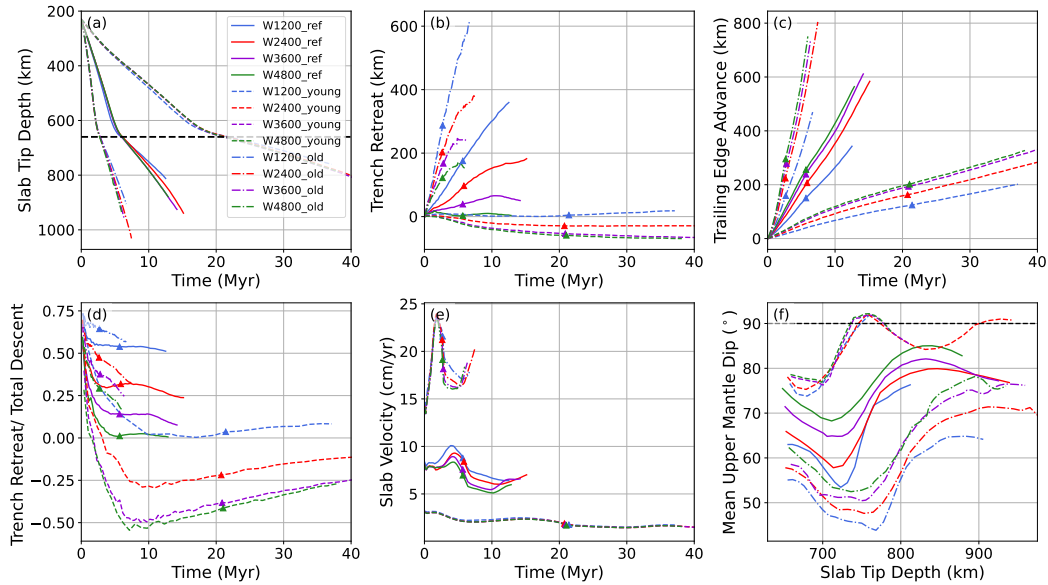


Figure 4. Comparison between all simulations: (a) slab tip depth, as a function of time, where the upper–lower mantle boundary is indicated by the black dotted line at 660 km depth; (b) amount of trench retreat; (c) amount of plate advance, measured at the plate’s trailing edge; (d) ratio of trench retreat to total length of plate subducted, which is the sum of trench retreat and trailing edge advance; (e) slab sinking velocity; and (f) average slab dip in the upper mantle, with the black dashed line indicating a vertical slab with dip angle of 90° . Triangles indicate the time where the slab tip starts interacting with the base of the upper mantle at 660 km depth. All measurements are taken at the symmetry plane.

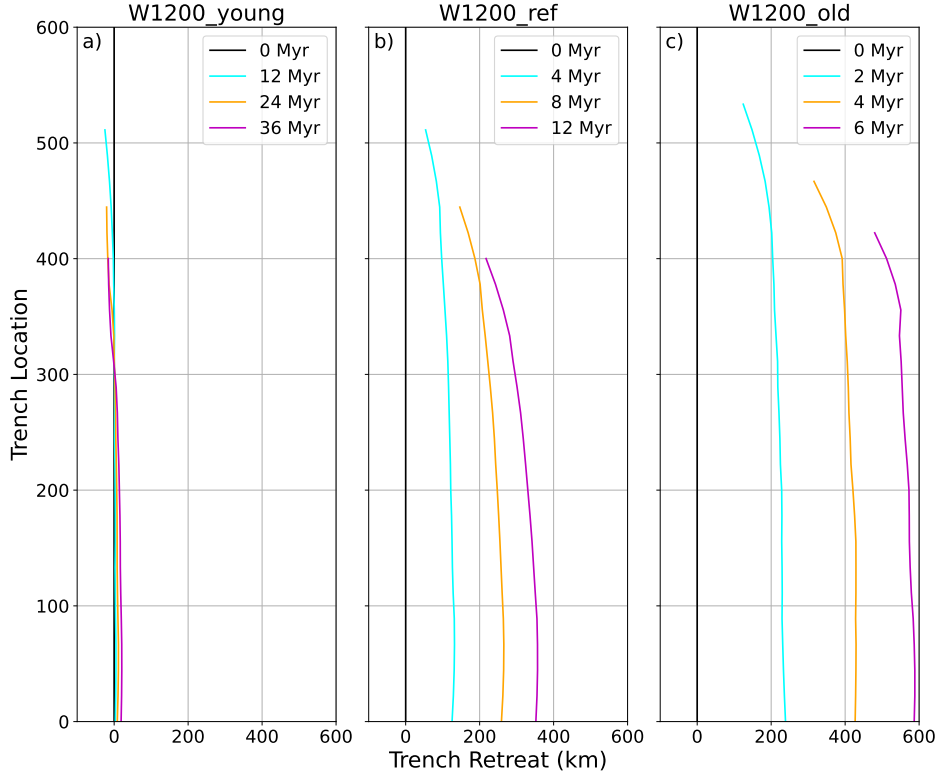


Figure 5. Spatio-temporal evolution of trench location of cases with a plate width of 1200 km. Times given in Myr since simulation initiation. (a) young: $H = 45$ km, $\Delta\rho = 40$ kg m $^{-3}$; (b) reference: $H = 70$ km, $\Delta\rho = 80$ kg m $^{-3}$; (c) old: $H = 100$ km, $\Delta\rho = 120$ kg m $^{-3}$.

286 is the strongest: it sinks faster, has a shallower upper mantle subduction angle, and drives
 287 significant trench retreat, with more than half of the subduction accommodated via this
 288 retreat (Figure 4). This case falls into the weak retreat regime (e.g., Schellart, 2008; Stegman,
 289 Farrington, et al., 2010; Garel et al., 2014; Goes et al., 2017). As expected, the reference
 290 case has an intermediate strength, with sinking and trench-retreat rates, in addition to
 291 the slab dip angle, all between those of the older and younger cases (Figure 4). As trench
 292 retreat accounts for slightly more than $\sim 50\%$ of the total subduction in the reference
 293 case, it also falls into the weak retreat regime.

294 3.3 Effect of subducting plate width

295 We next examine cases with the same buoyancy and strength combinations as in
 296 the previous section, but at larger widths of 2400 km, 3600 km and 4800 km.

297 3.3.1 Trench retreat

298 For cases that share a common plate age, a larger plate width reduces trench re-
 299 treat. As the slab tries to maintain its sinking rate, this results in stronger bending at
 300 the trench. The dynamical behaviour can lead to a shift in subduction regime, especially
 301 at the centre of the plate, where increased slab width causes slabs to steepen at the trench,
 302 with the trench sometimes advancing. The behaviour at the centre of the plate thereby
 303 shifts towards a ‘bending mode’, where slab bending at the trench takes up a significant
 304 part of the potential energy of the slab, as opposed to a ‘sinking mode’, where bending

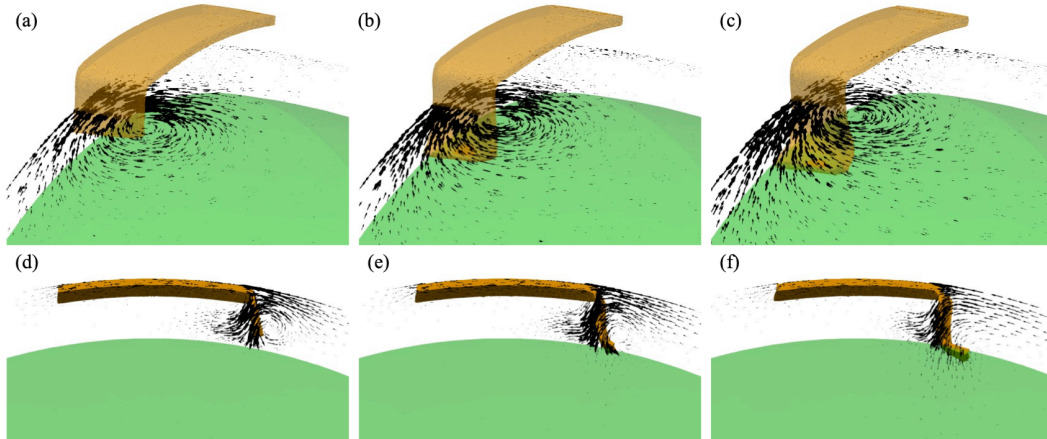


Figure 6. Snapshots of upper mantle flow regime for a plate width of 1200 km, of reference age (plate thickness of 70 km and $\Delta\rho$ of 80 kg m^{-3}). (a)-(c) Flow tangential to the radial direction at 300 km depth, highlighting the toroidal flow cell at the edge of the plate. The largest arrows represent a tangential velocity magnitude of 3.7 cm/yr (radial component of velocity removed); (b)-(d) Corresponding poloidal flow cells, in the mantle wedge and sub-slab regions. The largest arrow in the bottom panels represents a velocity magnitude of 9.4 cm/yr. As the slab tip interacts with the mantle transition zone, the poloidal cell diminishes as the viscosity increase in the lower mantle hampers return flow beneath the slab tip.

305 at the trench uses only 10-20% of the potential energy, and slab sinking is, in part, achieved
 306 through trench retreat (e.g. Capitanio et al., 2007; Ribe, 2010).

307 For younger cases, at all widths (W2400_young, W3600_young and W4800_young),
 308 slabs stretch and sink steeply in the upper mantle, at a dip of $> 75^\circ$ (Figures 4f), even-
 309 tually buckling upon interaction with the transition zone at 660 km depth, like their nar-
 310 rower counterpart (Figure 7). However, as plate width increases, the rate of trench ad-
 311 vance also increases. Upon interaction with the upper-lower mantle boundary, the 1200 km-
 312 wide cases display minimal trench motion, whereas the trench has advanced ~ 30 km,
 313 ~ 50 km and ~ 50 km for the 2400 km, 3600 km and 4800 km wide cases, respectively
 314 (Figure 4b). This folding, with some advance, is a characteristic of a ‘fold-and-retreat’
 315 bending mode (e.g., Schellart, 2008; Stegman, Farrington, et al., 2010; Goes et al., 2017),
 316 and the centre of wide young slabs display behaviour between a vertical folding and fold-
 317 and-retreat mode.

318 For wider cases at the reference age (W2400_ref, W3600_ref and W4800_ref), slabs
 319 retreat prior to interacting with the base of the upper mantle. At the symmetry plane,
 320 they steepen and buckle following interaction, thus exhibiting stronger bending at the
 321 trench in comparison to the 1200 km-wide case, which displayed a deflect-and-sink be-
 322 haviour (Figure 3a). As plate width increases, the upper mantle portion of the slab steep-
 323 ens (Figures 4f, 7). Buckled slabs with a width of 4800 km have maximum dips that ex-
 324 ceed those of the 2400 km wide case by $\sim 4^\circ$. At the symmetry plane, the trench retreat:total
 325 subduction ratio decreases with plate width (~ 0.5 , ~ 0.25 , ~ 0.1 , and ~ 0 for 1200 km,
 326 2400 km, 3600 km and 4800 km wide cases respectively – Figure 4d), indicating less of
 327 a role for trench retreat in accommodating subduction. This is most clearly demonstrated
 328 for the W4800_ref simulation, which transitions from retreat at a width of 1200 km, to
 329 stagnation at a width of 4800 km (Figures 4d).

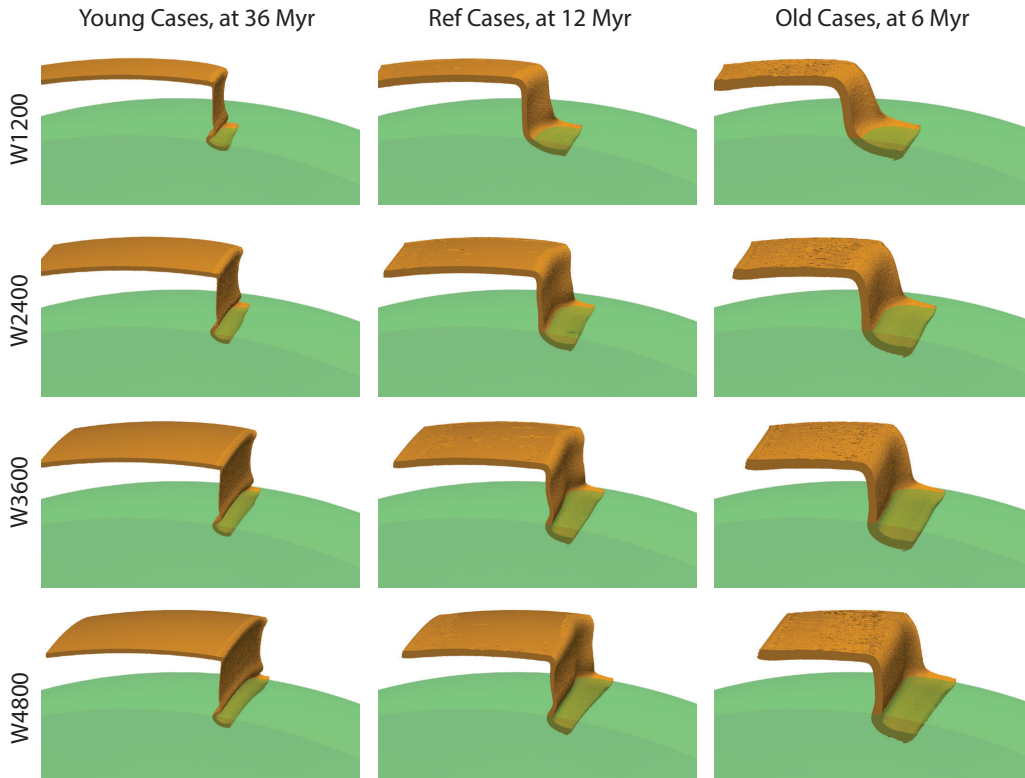


Figure 7. Final stage of model slab morphology. From top to bottom, models with plate widths of 1200 km, 2400 km, 3600 km, and 4800 km are shown, respectively. From left to right, we show the young cases at 36 Myr, reference cases at 12 Myr, and old cases at 6 Myr, respectively.

330 For older cases at widths of 2400 km (W2400_old), 3600 km (W3600_old), and 4800 km
 331 (W4800_old), slabs sink with shallower angles than corresponding reference age cases in
 332 the upper mantle (Figures 4f, 7), deflecting at transition zone depths and, subsequently,
 333 sinking through into the lower mantle. As plate width increases from 1200 km to 4800 km,
 334 the maximum upper mantle dip angle increases by $\sim 14^\circ$. The trench retreat:total sub-
 335 duction ratio also decreases as slab width increases, from ~ 0.6 to ~ 0.3 to ~ 0.25 to
 336 < 0.2 for 1200 km, 2400 km, 3600 km and 4800 km wide slabs, respectively. While the
 337 older cases across all widths fall into the weak retreat regime, the wider cases (W3600_old
 338 and W4800_old) exhibit a significant reduction in trench retreat post interaction with
 339 the transition zone (Figures 4b).

340 Taken together, our results demonstrate that as plate width increases, slabs dis-
 341 play less of a tendency to retreat across all three ages examined. As a consequence, they
 342 bend more strongly at the trench.

343 **3.3.2 Trench curvatures and along strike variations in morphology**

344 Different trench shapes are observed across the simulations examined, which can
 345 be categorised into 3 types: (i) ‘T’-type, where the trench is reasonably straight (e.g., Fig-
 346 ure 5a); (ii) ‘C’-type, where trench retreat is strongest in the centre of the slab relative
 347 to its edges (e.g., Figure 5b); and (iii) ‘W’-type, where trench retreat is low in the cen-

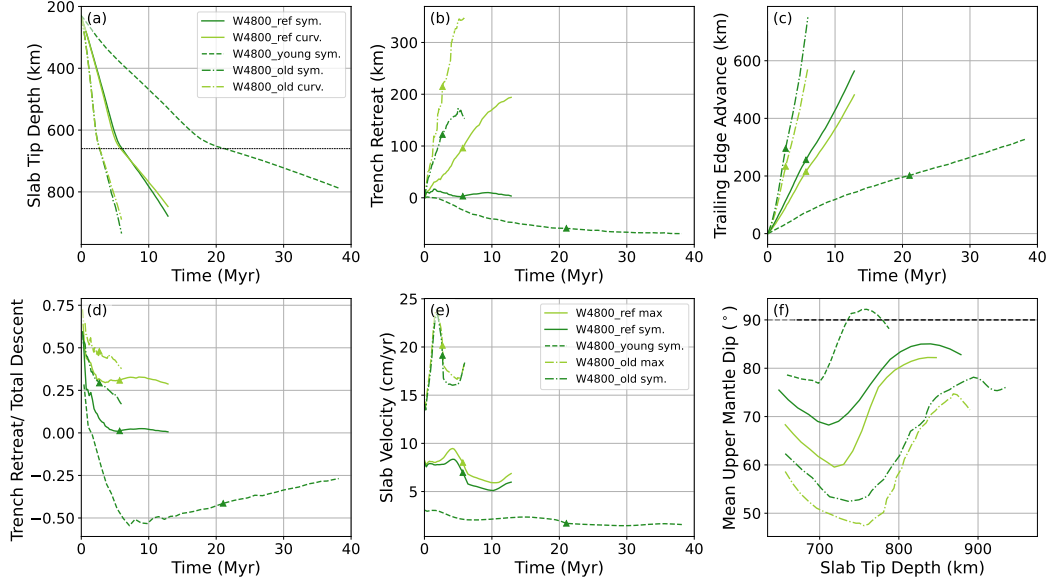


Figure 8. Comparison between simulations with a plate width of 4800 km. Measurements are taken at the centre of the slab (i.e., the symmetry plane, abbreviated to sym.) and the location of most trench retreat, which is at the centre of the concave curvature (curv.). (a) slab tip depth, as a function of time, where the upper–lower mantle boundary is indicated by the black dotted line at 660 km depth; (b) amount of trench retreat; (c) amount of plate advance, measured at the plate’s trailing edge; (d) ratio of trench retreat to total length of plate subducted, which is the sum of trench retreat and trailing edge advance; (e) slab sinking velocity at the symmetry plane, and the maximum down-going radial velocity (abbreviated to max); and (f) average slab dip in the upper mantle, with the black dashed line indicating a vertical slab with dip angle of 90° . Triangles indicate the time of slab tip interaction with the upper-lower mantle interface.

348
349

tre of the slab and at the edges, and higher in between (‘S’ curvature in half-width, as shown in Figure 11b).

350
351
352
353
354
355
356
357
358
359
360
361
362
363
364
365

We find that ‘I’-type trenches develop for younger cases across all plate widths: trenches remain reasonably straight, aside from a slight curvature adjacent to the slab edge (Figures 5a, 9a, 10a and 11a). ‘C’-type trenches develop for narrow plates that are retreating, for example, in cases W1200_ref and W1200_old (Figure 5b,c). For stronger plates that have moderate width, such as case W2400_old (Figure 9b), the trench develops a gentle curvature close to the edge, but the bulk of the trench remains approximately straight throughout the simulation, in an elongated ‘C’ shape. As slab width increases, ‘W’-type trenches develop in slabs that would have ‘C’-type trenches at a narrower width. This can be seen by comparing cases W2400_ref, W3600_ref and W4800_ref. Case W2400_ref develops a concave curvature at the edges, with the centre of the trench retreating slightly less than the edge (Figure 9b), placing it at the transition between ‘C’- and ‘W’-type trenches. Conversely, case W3600_ref and case W4800_ref display a ‘W’-type curvature (Figure 10b and Figure 11b). Similarly, for older slabs, wider trenches develop into a ‘W’ shape (‘S’ in half-width in Figure 11c). In case W4800_old, the curvature increases following slab transition-zone interaction and the difference in trench retreat between the centre and the region of most retreat also increases (Figure 8b).

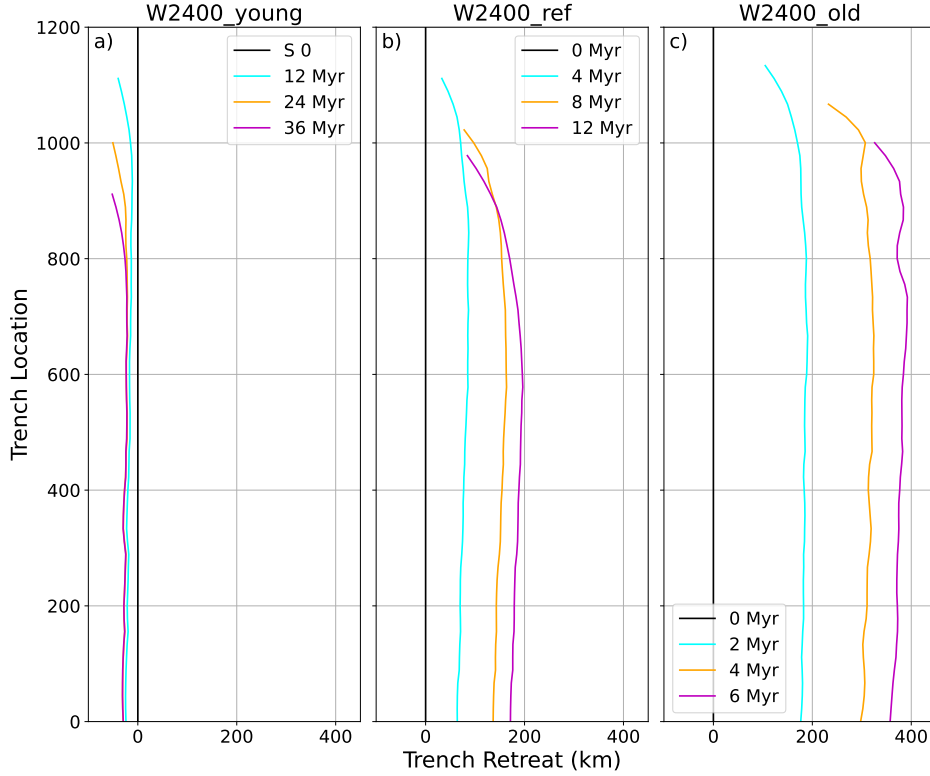


Figure 9. Spatio-temporal evolution of trench location in simulations with a plate width of 2400 km. Times given in Myr since simulation initiation. (a) young: $H = 45$ km, $\Delta\rho = 40$ kg m $^{-3}$; (b) reference: $H = 70$ km, $\Delta\rho = 80$ kg m $^{-3}$; (c) old: $H = 100$ km, $\Delta\rho = 120$ kg m $^{-3}$.

366 Taken together, our results demonstrate that the evolution of trench shape is de-
 367 pendent on both slab age and slab width. Younger and weaker slabs that are in the ver-
 368 tical folding regime develop mostly straight ‘I’-type trenches, regardless of slab width.
 369 For older cases that can drive trench retreat, trench curvatures evolve from a ‘C’-shape
 370 in narrower plates to a ‘W’-shape in wider plates, with slabs of greater strength tran-
 371 sitioning to a ‘W’ shape at a greater width.

372 Slab morphologies evolve with trench shape. For weaker cases with an ‘I’-type trench,
 373 subducting slab morphology is relatively uniform along strike (Figure 12a). For stronger
 374 wide retreating cases that develop a ‘W’-type trench, along-strike variations in trench
 375 retreat translate into morphological variations at depth (Figures 12b,c and 8a): at the
 376 symmetry plane, the slab is steep and buckles at the transition zone, with dips up to 9°
 377 larger than in the slab at the location of most retreat, where the slab deflects at transition-
 378 zone depths (Figure 8d,f).

379 4 Discussion

380 4.1 Role of Subducting Plate Age and Width

381 Our results demonstrate that the evolution of subduction systems is strongly sensi-
 382 tive to slab age (due to its effect on buoyancy and strength), which is consistent with
 383 several previous studies (e.g., Capitanio et al., 2007; Schellart, 2008; Stegman, Farring-
 384 ton, et al., 2010; Garel et al., 2014). Slabs with greater negative buoyancy and slab pull

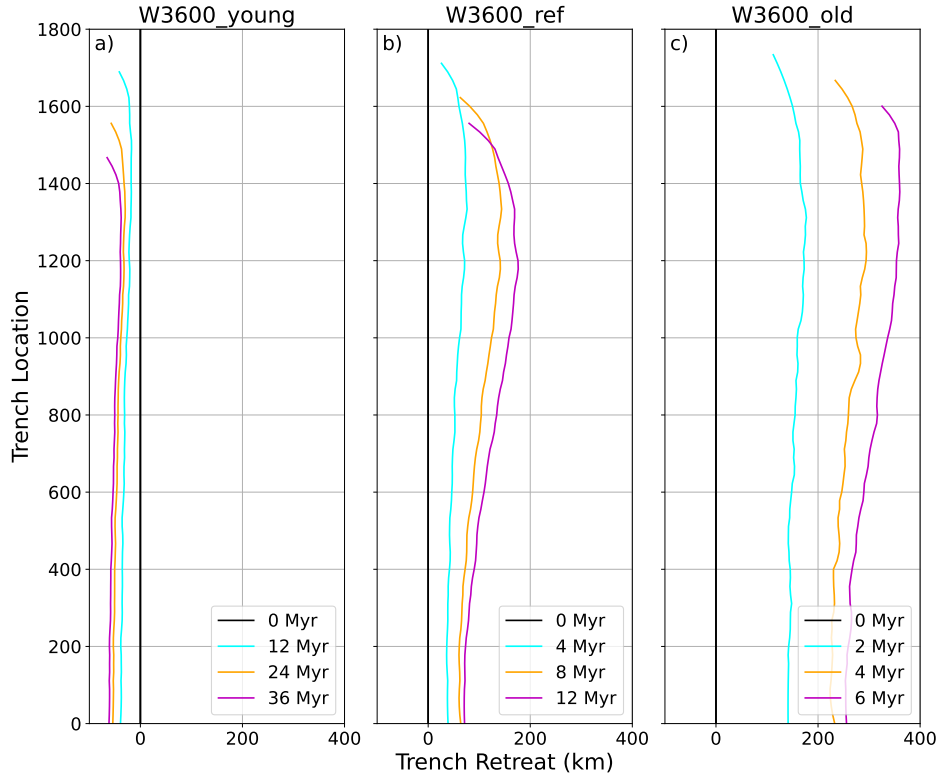


Figure 10. Spatio-temporal evolution of trench location in simulations with a plate width of 3600 km. Times given in Myr since simulation initiation. (a) young: $H = 45$ km, $\Delta\rho = 40$ kg m $^{-3}$; (b) reference: $H = 70$ km, $\Delta\rho = 80$ kg m $^{-3}$; (c) old: $H = 100$ km, $\Delta\rho = 120$ kg m $^{-3}$.

385 promote increased upper mantle sinking velocities (e.g., Stegman, Farrington, et al., 2010;
 386 Garel et al., 2014; Goes et al., 2017). Slab thickness determines slab strength (alongside
 387 buoyancy), with thicker slabs possessing a higher bending resistance (e.g., Conrad & Hager,
 388 1999; Bellahsen et al., 2005; Ribe, 2010; Capitanio & Morra, 2012) and, accordingly, tak-
 389 ing longer to bend at the trench. The regime that a subduction system falls into depends
 390 on a delicate balance between the amount of time taken to bend (larger for thicker slabs)
 391 and the sinking time (larger for younger slabs) (Ribe, 2010). Taken together, in younger
 392 slabs (low slab pull – longer sinking times; low slab strength – shorter bending times),
 393 bending dominates over trench retreat, with slabs typically subducting steeply and buck-
 394 ling upon interaction with the upper-lower mantle boundary, owing to the high angle of
 395 incidence. Conversely, in older slabs (high slab pull – shorter sinking times; high slab strength
 396 – longer bending times), there is insufficient time for substantial bending at the trench,
 397 with subduction accommodated principally through trench retreat. As a result, slabs
 398 typically exhibit a shallower upper mantle dip angle, which facilitates slab deflection and
 399 stagnation at the base of the upper mantle (e.g., Torii & Yoshioka, 2007; Čížková & Bina,
 400 2013; Garel et al., 2014; Agrusta et al., 2017).

401 The evolution of ‘C’- and ‘W’-shaped trenches for our retreating cases are similar
 402 to results from Schellart et al. (2007), with curvature at slab edges induced by toroidal
 403 flow around and into the slab. Interplay between the size and strength of the toroidal
 404 cell, the width of the slab, and the slab’s resistance to along-strike bending, dictate how
 405 trench shape responds. The size of the toroidal cell determines over what region along
 406 the trench the plate experiences significant force from the adjacent mantle flow and, hence,

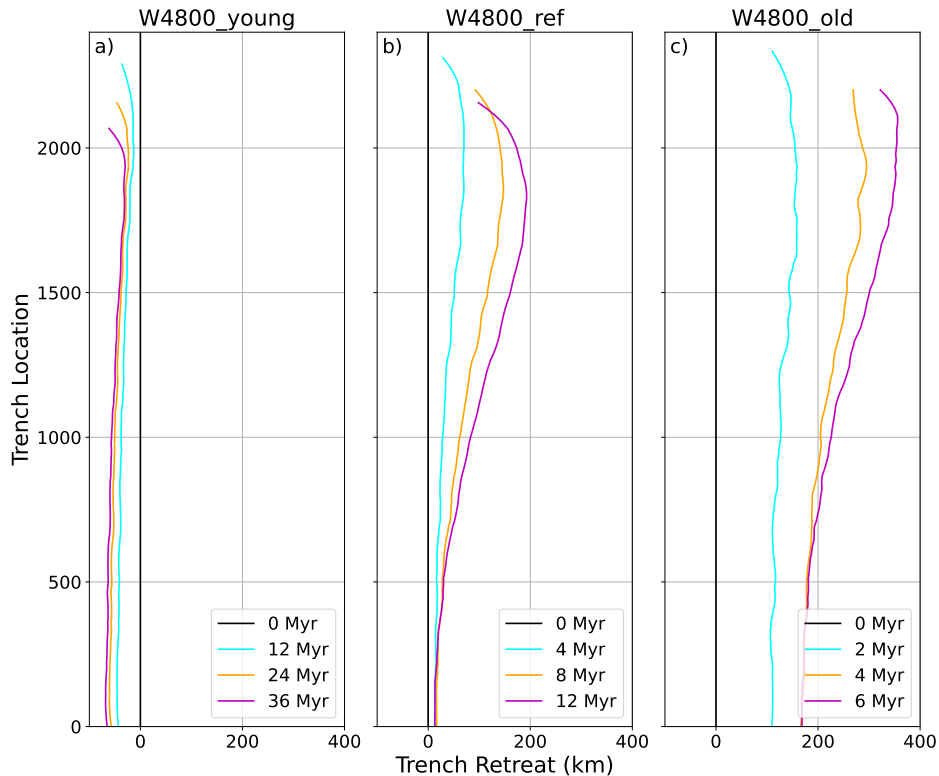


Figure 11. Spatio-temporal evolution of trench location in simulations with a plate width of 4800 km. Times given in Myr since simulation initiation. (a) young: $H = 45$ km, $\Delta\rho = 40$ kg m $^{-3}$; (b) reference: $H = 70$ km, $\Delta\rho = 80$ kg m $^{-3}$; (c) old: $H = 100$ km, $\Delta\rho = 120$ kg m $^{-3}$.

407 the location of potential concave curvature development. The strength of the toroidal
 408 cell is determined by the amount of trench retreat. The width of the plate relative to
 409 the size of the toroidal cell determines the distance between the toroidal cells at both
 410 edges. When these factors are coupled with the plate's resistance to bending, the evolu-
 411 tion of trench shape can be understood. 'C'-shaped trenches are observed for narrow
 412 plates, where toroidal cell sizes are close to half of the slab width (Figure 6). 'W'-shaped
 413 trenches are observed for wider plates, where the size of the toroidal cell is substantially
 414 smaller than the width of the plate: the centre of such plates are thus not markedly in-
 415 fluenced by toroidal flow (Figure 13a). Plates with less resistance to bending along strike
 416 can develop enhanced curvature at the trench (W3600_ref, Figure 10b); conversely, plates
 417 with a higher strength can prevent significant curvature development at the trench, re-
 418 maining in a relatively uniform elongated 'C'-shape rather than evolving into a 'W'-shape
 419 (e.g., W3600_old, Figure 10c).

420 While the influence of plate width on subduction dynamics has been studied pre-
 421 viously (e.g., Stegman et al., 2006; Schellart et al., 2007; Di Giuseppe et al., 2008), our
 422 results demonstrate that the important role of width is strongly modulated by the age
 423 of the plate and its effect on plate strength. The change from a 'C'-shaped trench to a
 424 'W'-shaped trench with increasing width only occurs for cases that are initially in a re-
 425 treating regime (i.e., older plates). For younger plates that are in the vertical folding regime,
 426 increasing plate width has little impact on along-strike variability, because these plates
 427 do not subduct through trench retreat and, hence, cannot generate toroidal cells of the

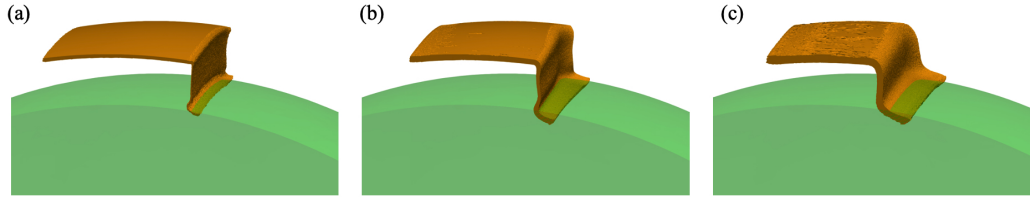


Figure 12. 3-D morphology of cases with different ages at a width of 4800 km: (a) young: $H = 45$ km, $\Delta\rho = 40$ kg m $^{-3}$; (b) reference: $H = 70$ km, $\Delta\rho = 80$ kg m $^{-3}$; (c) old: $H = 100$ km, $\Delta\rho = 120$ kg m $^{-3}$. Young cases have relatively uniform morphology along-strike, whereas older cases (b,c) display varying morphologies: vertically folding at the centre, but horizontally deflecting closer to the edge.

428 intensity required to induce trench deformation (Figure 13b). Accordingly, the younger
429 cases develop ‘I’-type trench shapes across all widths examined in this study.

430 Variations in the amount of trench retreat also translate into along-strike morpho-
431 logical variations at depth. These variations can also be understood by the along-strike
432 influence of toroidal flow, facilitating trench retreat. Vertical folding morphologies cor-
433 respond to (parts of the) slabs with limited trench retreat or minor advance, while re-
434 treating segments lead to shallower dips and deflection at the base of the upper man-
435 tle. While all wide slabs display the typical morphology of the vertical folding regime
436 at the centre, the young models have tight buckles, whereas older slabs have open folds
437 with larger bending radii. This difference in bending radii illustrates that older slabs have
438 higher bending resistance and strength than younger slabs, despite falling into the same
439 subduction regime. Overall, as plate width increases, the center of the slab shifts from
440 sinking to bending, due to the lack of toroidal flow and its role in driving trench retreat.

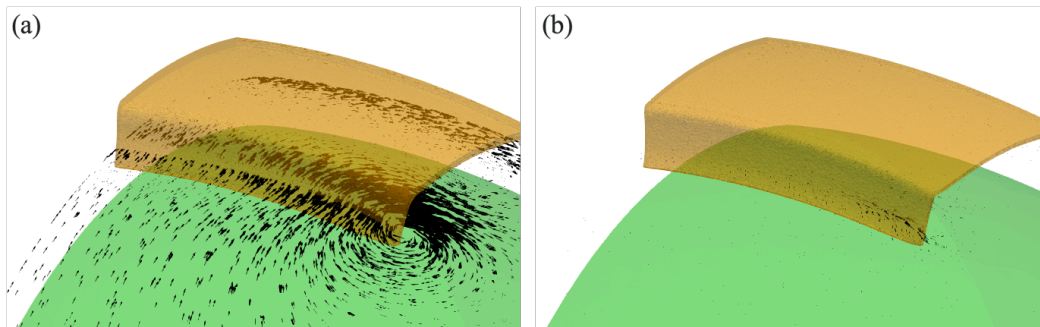


Figure 13. Lateral flow patterns at 300 km depth for: (a) case W4800_ref; and (b) case W4800_young. The length and direction of the arrows illustrates the magnitude and direction of tangential velocities (i.e. after the radial component has been removed). In both panels, the largest arrow represents a tangential velocity magnitude of 2.5 cm/yr. For the reference age case in (a), a toroidal cell can be identified at the edge of the slab, which does not extend to the centre of the slab. For the younger case in (b), although there is some toroidal flow around the edge of the slab, its magnitude and area of influence is insignificant when compared to the reference case.

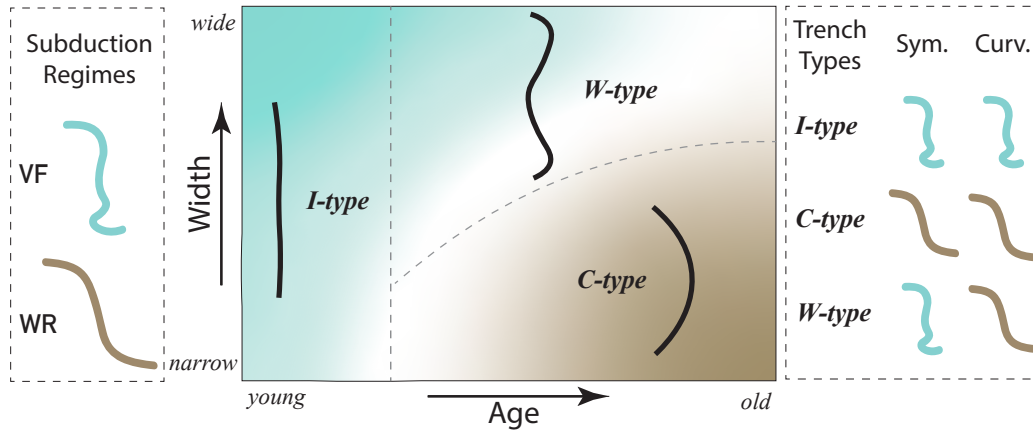


Figure 14. Schematic diagrams of how age and width, affect subduction styles and trench shape. Regimes: VF - vertical folding; WR - weak retreat. The three trench types ‘I’, ‘C’ and ‘W’ are separated into three approximate domains, by gray dashed lines, with slabs that lie on domain boundaries at the transition between two trench types. Slab behaviours that are in VF at the symmetry plane are represented by the cyan region, and those in WR are represented by the brown region. The rightmost panel illustrates the slab morphology at the centre of the slab (i.e., the symmetry plane, abbreviated to sym.) and the location of most trench retreat, which is at the centre of the concave curvature (curv.). For young plates, the subduction regime is VF regardless of the width of the plate, and trench shapes are mostly straight, indicated by ‘I’-type. As age increases, it is easier to drive trench retreat and slabs fall into the WR regime; but as width increases, the centre of the plate shifts towards the VF regime. Beyond a certain age, the narrower and/or older plates tend to develop ‘C’-type trenches; wider and/or younger plates tend to develop ‘W’-type trenches.

441 The competing roles of plate age and plate width in dictating the subduction style are
 442 summarised via a regime diagram in Figure 14.

443 4.2 Implications for Subduction on Earth

444 Our model predictions across different plate ages and widths, can be used to analyse
 445 how these aspects combine to control the spatio-temporal evolution of trenches on
 446 Earth. While Earth’s subduction zones are substantially more complex than those con-
 447 sidered in our simulations, due to a multitude of factors including subducting plates of
 448 non-uniform age, the subduction of buoyant anomalies, and the influence of overriding
 449 plates, the ‘I’, ‘C’ and ‘W’ trench shapes predicted by our models are consistent with
 450 present-day trench shapes (e.g. Bird, 2003; Schellart et al., 2007; Heuret et al., 2011) and
 451 those in reconstructions of plate motion histories through the Cenozoic Era (Müller et
 452 al., 2016, 2019).

453 4.2.1 ‘I’-type Trenches

454 Our results demonstrate that ‘I’-shape trenches typically develop when a young plate
 455 subducts with negligible trench motion, regardless of trench width. The tectonic recon-
 456 structions of Müller et al. (2019) provide some examples of young plate subduction dur-
 457 ing the Cenozoic, such as the subduction of the Izanagi plate at the Japan trench at 50–

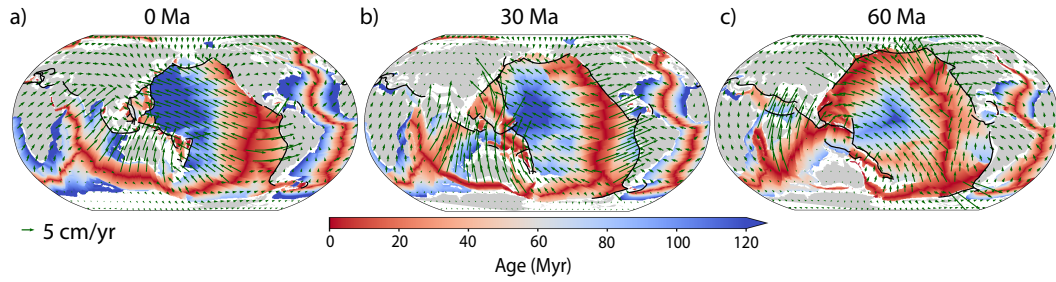


Figure 15. Maps of ocean-floor age and trench positions (black lines) based on the plate reconstruction by Müller et al. (2019) at: (a) the present-day; (b) 30 Ma; and (c) 60 Ma. Green arrows represent plate velocity (in the mantle reference frame of the reconstruction). For reference, present day coastlines are shown in light grey.

458 60 Ma and the subduction of the Farallon plate below North America prior to ~ 30 Ma
 459 (Figure 15).

460 As illustrated in Figure 16, the Japan subduction zone was relatively straight (apart
 461 from its northern end) with minimal trench motion between 50 and 60 Ma, character-
 462 istics typical of ‘I’-type trenches. The trench measured ~ 5000 km in width, and a young
 463 plate (~ 10 Myr) was subducted along the whole trench (Figure 15c). As time advanced
 464 past 50 Ma, the main part of the trench evolved from an ‘I’-type towards a ‘C’-type ex-
 465 ample, with increasing trench retreat, trench curvature and trench segmentation (Fig-
 466 ure 16a). This is coincident with an increase in subducting plate age, as shown in Fig-
 467 ure 15(a,b), after the subduction of the Izanagi-Pacific ridge at ~ 50 Ma (Kimura et al.,
 468 2019).

469 Similarly, the reconstructed North America trench displayed an ‘I’-type shape prior
 470 to 30 Ma, when the very young (~ 10 Myr at 30 Ma) Farallon plate was subducting be-
 471 neath North America, as shown in Figure 15(b). Prior to 30 Ma, the trench shape was
 472 relatively straight, with very little trench retreat, particularly from 30–50 Ma (Figure

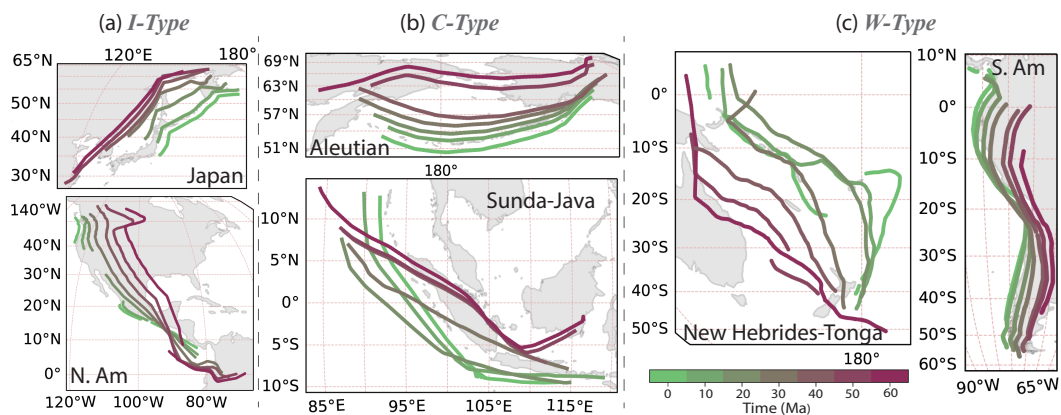


Figure 16. Examples of ‘I’ shape (a), ‘C’ shape (b) and ‘W’ shape (c) trenches based on the plate reconstruction by Müller et al. (2019), where trenches are drawn at 10 Myr intervals. N.Am - North America; S.Am - South America.

473 16). Following breakup of the Farallon Plate in the mid-Cenozoic, into the Juan de Fuca,
 474 Cocos and Nazca Plates (e.g., Atwater, 1970; Lonsdale, 2005), the continuity of the 5900 km-
 475 wide trench was lost, and the strike-slip San Andreas Fault developed on the west coast
 476 of North America.

477 **4.2.2 ‘C’-type Trenches**

478 Our results suggest that ‘C’-shape trenches should be associated with moderate to
 479 old subducting plate ages and moderate slab widths. ‘C’-shape trenches are the most
 480 common trench shape observed on Earth. The Aleutian subduction zone and the Sunda-
 481 Java subduction zone are two examples of ‘C’-shape trenches that developed during the
 482 Cenozoic (Figure 16). Although both trenches have also been affected by buoyant struc-
 483 tures on the incoming plate (such as the Yakutat terrane below Alaska and Australian
 484 continental crust impinging on the Banda part of the Sunda-Java arc), we propose that
 485 the combined width and age of the downgoing plate exerted an important control on the
 486 evolution of trench shape.

487 The Aleutian trench extends ~ 4000 km from the south coast of Alaska to Kam-
 488 chatka (Scholl et al., 1975). Prior to 40 Ma, the Kula plate subducted at the eastern side
 489 of the Aleutian trench, and the Pacific plate subducted at the western side. Subduction
 490 of young oceanic lithosphere ($\sim 10 - 40$ Myr at 60 Ma) along the trench (Figure 15c)
 491 resulted in a gentle curvature, with a shape between ‘C’- and ‘I’-types (Figure 16, Müller
 492 et al., 2019). At 40 Ma, when the Pacific plate had started subducting at the Aleutian
 493 trench; the age of the subducting plate increased and the Aleutian trench retreated and
 494 developed a ‘C’-shape curvature, with enhanced curvature in the west (Figure 16). This
 495 is consistent with our modelling predictions, and could be related to the non-uniform sub-
 496 ducting plate age at the Aleutian trench: the subducting Pacific plate is younger to the
 497 east (currently ~ 10 Myr) and older to the west (~ 120 Myr at present, Figure 15a,b),
 498 with the older part of the plate driving more retreat, generating the asymmetric ‘C’-shaped
 499 trench.

500 The Sunda-Java trench also has a complex subduction history. Prior to 43 Ma, the
 501 active Wharton ridge was subducting beneath Sumatra, but since then the ridge has be-
 502 come inactive (Whittaker et al., 2007). As a result, the majority of material subducted
 503 prior to 43 Ma was young (~ 10 Myr old – Figure 15c), leading to minimal trench mo-
 504 tion at the Sunda-Java subduction zone, consistent with ‘I’-type subduction (Figure 16b).
 505 As the Wharton ridge ceased spreading and the subducting plate age increased (Figure
 506 15a,b), the trench began to retreat and developed a ‘C’ shape across its ~ 5000 km width,
 507 again demonstrating that an ‘I’-type to ‘C’-type transition can occur when subducting
 508 plate age increases, consistent with our modelling predictions.

509 **4.2.3 ‘W’-type Trenches**

510 ‘W’-type trenches develop with moderate and older subducting plate age and very
 511 wide trenches. The South American trench is the textbook example of a ‘W’-shape (Schellart
 512 et al., 2007): it exhibits concave curvature on both edges, with the centre of the trench
 513 almost stagnant throughout the Cenozoic (Figure 15c). Subduction in the South Pacific
 514 also exhibits ‘W’-type characteristics in the early Cenozoic.

515 The South American trench is over 6000 km long, and subducted moderately old
 516 material ($\sim 50 - 80$ Myr) throughout the Cenozoic at the centre of the trench (Figure
 517 15). Trench evolution shows increasing oroclinal bending through the Cenozoic (Schepers
 518 et al., 2017) and, hence, more retreat towards the north and south than in the central
 519 part at the Bolivian bend (Figure 16, Müller et al., 2019). The present-day trench shape
 520 is typical of our wide plate model predictions, where the Bolivian Orocline is located close
 521 to the centre of the trench, while sections of the trench close the edges have a concave

522 geometry. The subduction of pre-existing buoyant features on the Nazca Plate and in-
 523 teraction with varying thickness upper plate are further complexities that likely added
 524 to its evolution towards the current geometry (e.g., Gutscher, Olivet, et al., 1999; Es-
 525 purt et al., 2008; Capitanio et al., 2011). However, although it is likely that multiple fac-
 526 tors contribute to the shape of the trench at the South America Subduction Zone, our
 527 results agree with the previous suggestion by Schellart et al. (2007) that the first-order
 528 ‘W’-shape is dictated by its large width, modulated by its moderate subducting-plate
 529 age.

530 The South Pacific region has a relatively complex tectonic history. In the early Ceno-
 531 zoic, old Pacific plate was subducting under the South Pacific trench, which had length
 532 exceeding 6000 km (Figure 15c). The trench at 60 Ma has characteristics of a ‘W’-shape.
 533 There is a region of low trench retreat near 20° S, where the oldest (~ 100 Myr) part
 534 of the plate was subducting. The trench is concave north and south of this point. As the
 535 trench evolves, the northern and southern ends of it start to evolve separately, and the
 536 shorter trench takes on a ‘C’ type shape (Figure 16, 15c). Post 20 Ma, in response to ar-
 537 rival of the buoyant Ontong-Java plateau (Neal et al., 1997; Mann & Taira, 2004; Stotz
 538 et al., 2017) the trench segments further into the New Hebrides, New Britain and Tonga-
 539 Kermadec-Hikurangi trenches (e.g., Pelletier et al., 1998). These different stages of evo-
 540 lution and the shape of the resulting trenches were likely preconditioned by the origi-
 541 nal ‘W’ shape.

542 Overall, the examples of ‘I’-, ‘C’- and ‘W’-shape trenches on Earth are in line with
 543 our modeling results. ‘I’-type trenches are associated with very young downgoing plates
 544 of ~ 10 Myr old; and as plate age increases, some transition into ‘C’-shape trenches. ‘W’-
 545 shape trenches are observed in subduction zones exceeding 6000 km width, where older
 546 material (greater than 50 Myr old) is being subducted, thus driving trench retreat. There
 547 is no doubt that the trench shape at each subduction zone is further modulated by ad-
 548 ditional complexities, including variable downgoing plate age along strike, subduction
 549 of buoyant active or bathymetric ridges, variations in thickness and buoyancy of the up-
 550 per plate, and large tectonic reconfiguration events such as the India-Eurasian collision.
 551 Nonetheless, our results demonstrate the key role that both subducting plate age and
 552 width play in controlling the evolution of trench geometry, providing a framework to bet-
 553 ter understand the evolution of subduction zones.

544 5 Conclusions

555 We have presented new 3-D spherical free-subduction models with a composite visco-
 556 plastic plate and viscously layered mantle. We examined the sensitivity of subduction
 557 dynamics and trench evolution to plate age (simulated with covarying plate densities and
 558 thicknesses) and plate width.

559 Our results complement previous studies on the effect of age and width on the evo-
 560 lution of subduction zones. As plate age increases, plate strength increases and, as a re-
 561 sult, the subduction style transitions from vertically sinking and folding to retreating with
 562 a shallower upper mantle dip angle. Our models show a tendency to produce ‘C’ shaped
 563 trenches for narrower plates and ‘W’ shaped trenches for wider plates, consistent with
 564 the models of Schellart et al. (2007). However, we also find that the effect of width is
 565 modulated by the age of the subducting plate. For young plates that are in the verti-
 566 cal folding regime, the trench does not develop a ‘W’ shape, regardless of width. ‘C’ or
 567 ‘W’-shaped trenches are only generated in cases where the slab is able to drive trench
 568 retreat. For those cases that do retreat, younger and weaker plates develop enhanced along-
 569 strike variability in trench shape.

570 We now have the means to simulate subduction dynamics in a spherical shell ge-
 571 ometry, which is appropriate for Earth’s mantle. This opens up new possibilities and will

572 be used in the future to investigate additional factors that affect subduction dynamics
573 and their expression at Earth’s surface.

574 **Acknowledgments**

575 F.C. is funded by an Australian Government Research Training Program (RTP) Schol-
576 arship. D.R.D. acknowledges support from the Australian Research Council (ARC), un-
577 der DP170100058. L.S. was funded by an EPSRC DTP studentship (EP/N509486/1),
578 S.G. received support under NERC grant NE/K010743/1. Numerical simulations were
579 undertaken on the NCI National Facility in Canberra, Australia, which is supported by
580 the Australian Commonwealth Government. The Fluidity computational modelling frame-
581 work, including source code and documentation, is available from [https://fluidityproject](https://fluidityproject.github.io/)
582 [.github.io/](https://fluidityproject.github.io/); the version used for the simulations presented herein has been archived
583 at <https://zenodo.org/record/5636819#.YYBeydZBxR4>. Authors would like to thank
584 Cian Wilson, Chris Matthews, Thomas Duvernay, Siavash Ghelichkhan, Angus Gibson
585 and Marthe Klöcking for fruitful discussions at various stages of this research.

586 **References**

- 587 Agrusta, R., Goes, S., & van Hunen, J. (2017). Subducting-slab transition-zone
588 interaction: Stagnation, penetration and mode switches. *Earth and Planetary*
589 *Science Letters*, *464*, 10–23.
- 590 Alsaif, M., Garel, F., Gueydan, F., & Davies, D. R. (2020). Upper plate deformation
591 and trench retreat modulated by subduction-driven shallow asthenospheric
592 flows. *Earth and Planetary Science Letters*, *532*, 116013.
- 593 Atwater, T. (1970). Implications of plate tectonics for the Cenozoic tectonic evolu-
594 tion of western North America. *Geological Society of America Bulletin*, *81*(12),
595 3513–3536.
- 596 Balay, S., Abhyankar, S., Adams, M. F., Brown, J., Brune, P., Buschelman, K.,
597 ... Zhang, H. (2021a). *PETSc users manual* (Tech. Rep. No. ANL-
598 95/11 - Revision 3.15). Argonne National Laboratory. Retrieved from
599 <https://www.mcs.anl.gov/petsc>
- 600 Balay, S., Abhyankar, S., Adams, M. F., Brown, J., Brune, P., Buschelman, K., ...
601 Zhang, H. (2021b). *PETSc Web page*. <https://www.mcs.anl.gov/petsc>.
602 Retrieved from <https://www.mcs.anl.gov/petsc>
- 603 Balay, S., Gropp, W. D., McInnes, L. C., & Smith, B. F. (1997). Efficient manage-
604 ment of parallelism in object-oriented numerical software libraries. In *Modern*
605 *software tools for scientific computing* (pp. 163–202). Birkhauser Boston Inc.
- 606 Bayly, B. (1982). Geometry of subducted plates and island arcs viewed as a buckling
607 problem. *Geology*, *10*(12), 629–632.
- 608 Beall, A., Fagereng, Å., Davies, J. H., Garel, F., & Davies, D. R. (2021). Influence of
609 subduction zone dynamics on interface shear stress and potential relationship
610 with seismogenic behavior. *Geochemistry, Geophysics, Geosystems*, *22*(2),
611 e2020GC009267.
- 612 Becker, T. W., & Faccenna, C. (2011). Mantle conveyor beneath the tethyan colli-
613 sional belt. *Earth and Planetary Science Letters*, *310*(3-4), 453–461.
- 614 Bellahsen, N., Faccenna, C., & Funicello, F. (2005). Dynamics of subduction and
615 plate motion in laboratory experiments: Insights into the “plate tectonics” be-
616 havior of the Earth. *Journal of Geophysical Research: Solid Earth*, *110*(B1).
- 617 Bird, P. (2003). An updated digital model of plate boundaries. *Geochemistry, Geo-*
618 *physics, Geosystems*, *4*(3).
- 619 Butterworth, N. P., Quevedo, L., Morra, G., & Müller, R. (2012). Influence of over-
620 riding plate geometry and rheology on subduction. *Geochemistry, Geophysics,*
621 *Geosystems*, *13*(6).
- 622 Butterworth, N. P., Talsma, A. S., Müller, R. D., Seton, M., Bunge, H.-P., Schu-

- 623 berth, B. S. A., ... Heine, C. (2014). Geological, tomographic, kinematic
624 and geodynamic constraints on the dynamics of sinking slabs. *Journal of*
625 *Geodynamics*, 73, 1–13.
- 626 Capitanio, F. A., Faccenna, C., Zlotnik, S., & Stegman, D. R. (2011). Subduction
627 dynamics and the origin of Andean orogeny and the Bolivian orocline. *Nature*,
628 480(7375), 83–86.
- 629 Capitanio, F. A., & Morra, G. (2012). The bending mechanics in a dynamic sub-
630 duction system: Constraints from numerical modelling and global compilation
631 analysis. *Tectonophysics*, 522, 224–234.
- 632 Capitanio, F. A., Morra, G., & Goes, S. (2007). Dynamic models of downgoing
633 plate-buoyancy driven subduction: Subduction motions and energy dissipation.
634 *Earth and Planetary Science Letters*, 262(1-2), 284–297.
- 635 Capitanio, F. A., Stegman, D. R., Moresi, L. N., & Sharples, W. (2010). Upper plate
636 controls on deep subduction, trench migrations and deformations at convergent
637 margins. *Tectonophysics*, 483(1-2), 80–92.
- 638 Chamolly, A., & Ribe, N. M. (2021). Fluid mechanics of free subduction on a
639 sphere. part 1. the axisymmetric case. *Journal of Fluid Mechanics*, 929.
- 640 Čížková, H., & Bina, C. R. (2013). Effects of mantle and subduction-interface rhe-
641 ologies on slab stagnation and trench rollback. *Earth and Planetary Science*
642 *Letters*, 379, 95–103.
- 643 Čížková, H., & Bina, C. R. (2015). Geodynamics of trench advance: Insights from a
644 philippine-sea-style geometry. *Earth and Planetary Science Letters*, 430, 408–
645 415.
- 646 Čížková, H., & Bina, C. R. (2019). Linked influences on slab stagnation: Interplay
647 between lower mantle viscosity structure, phase transitions, and plate coupling.
648 *Earth and Planetary Science Letters*, 509, 88–99.
- 649 Čížková, H., van Hunen, J., & van den Berg, A. (2007). Stress distribution within
650 subducting slabs and their deformation in the transition zone. *Physics of the*
651 *Earth and Planetary Interiors*, 161(3-4), 202–214.
- 652 Čížková, H., van Hunen, J., van den Berg, A. P., & Vlaar, N. J. (2002). The in-
653 fluence of rheological weakening and yield stress on the interaction of slabs
654 with the 670 km discontinuity. *Earth and Planetary Science Letters*, 199(3-4),
655 447–457.
- 656 Conrad, C. P., & Hager, B. H. (1999). Effects of plate bending and fault strength
657 at subduction zones on plate dynamics. *Journal of Geophysical Research: Solid*
658 *Earth*, 104(B8), 17551–17571.
- 659 Cross, T. A., & Pilger, R. H. (1982). Controls of subduction geometry, location of
660 magmatic arcs, and tectonics of arc and back-arc regions. *Geological Society of*
661 *America Bulletin*, 93(6), 545–562.
- 662 Davies, D. R., Le Voci, G., Goes, S., Kramer, S. C., & Wilson, C. R. (2016). The
663 mantle wedge’s transient 3-D flow regime and thermal structure. *Geochem.*
664 *Geophys. Geosys.*, 17, 78-100. doi: 10.1002/2015GC006125
- 665 Davies, D. R., Wilson, C. R., & Kramer, S. C. (2011). Fluidity: A fully unstructured
666 anisotropic adaptive mesh computational modeling framework for geodynam-
667 ics. *Geochemistry, Geophysics, Geosystems*, 12(6).
- 668 Di Giuseppe, E., van Hunen, J., Funicello, F., Faccenna, C., & Giardini, D. (2008).
669 Slab stiffness control of trench motion: Insights from numerical models. *Geo-*
670 *chemistry, Geophysics, Geosystems*, 9(2).
- 671 Espurt, N., Funicello, F., Martinod, J., Guillaume, B., Regard, V., Faccenna, C., &
672 Brusset, S. (2008). Flat subduction dynamics and deformation of the South
673 American plate: Insights from analog modeling. *Tectonics*, 27(3).
- 674 Faccenna, C., Becker, T. W., Lucente, F. P., Jolivet, L., & Rossetti, F. (2001). His-
675 tory of subduction and back arc extension in the Central Mediterranean. *Geo-*
676 *physical Journal International*, 145(3), 809–820.
- 677 Forsyth, D., & Uyeda, S. (1975). On the relative importance of the driving forces of

- 678 plate motion. *Geophysical Journal International*, *43*(1), 163–200.
- 679 Frank, F. (1968). Curvature of island arcs. *Nature*, *220*(5165), 363–363.
- 680 Fukao, Y., & Obayashi, M. (2013a). Subducted slabs stagnant above, penetrating
681 through and trapped below the 660 km discontinuity. *J. Geophys. Res.*, *118*,
682 5920–5938. doi: 10.1002/2013JB010466
- 683 Fukao, Y., & Obayashi, M. (2013b). Subducted slabs stagnant above, penetrating
684 through, and trapped below the 660 km discontinuity. *Journal of Geophysical
685 Research: Solid Earth*, *118*(11), 5920–5938.
- 686 Fukao, Y., Obayashi, M., Nakakuki, T., & Group, D. S. P. (2009). Stagnant slab: a
687 review. *Annual Review of Earth and Planetary Sciences*, *37*, 19–46.
- 688 Fukao, Y., Yamaoka, K., & Sakurai, T. (1987). Spherical shell tectonics: buckling
689 of subducting lithosphere. *Physics of the earth and planetary interiors*, *45*(1),
690 59–67.
- 691 Funicello, F., Faccenna, C., Heuret, A., Lallemand, S., Di Giuseppe, E., & Becker,
692 T. W. (2008). Trench migration, net rotation and slab–mantle coupling. *Earth
693 and Planetary Science Letters*, *271*(1-4), 233–240.
- 694 Funicello, F., Moroni, M., Piromallo, C., Faccenna, C., Cenedese, A., & Bui, H. A.
695 (2006). Mapping mantle flow during retreating subduction: Laboratory models
696 analyzed by feature tracking. *Journal of Geophysical Research: Solid Earth*,
697 *111*(B3).
- 698 Garel, F., Goes, S., Davies, D. R., Davies, J. H., Kramer, S. C., & Wilson, C. R.
699 (2014). Interaction of subducted slabs with the mantle transition-zone: A
700 regime diagram from 2-D thermo-mechanical models with a mobile trench and
701 an overriding plate. *Geochemistry, Geophysics, Geosystems*, *15*(5), 1739–1765.
- 702 Garel, F., Thoraval, C., Tommasi, A., Demouchy, S., & Davies, D. R. (2020). Using
703 thermo-mechanical models of subduction to constrain effective mantle viscos-
704 ity. *Earth and Planetary Science Letters*, *539*, 116243.
- 705 Goes, S., Agrusta, R., van Hunen, J., & Garel, F. (2017). Subduction-transition zone
706 interaction: A review. *Geosphere*, *13*(3), 644–664.
- 707 Goes, S., Capitanio, F. A., & Morra, G. (2008). Evidence of lower-mantle slab pen-
708 etration phases in plate motions. *Nature*, *451*(7181), 981–984.
- 709 Goes, S., Capitanio, F. A., Morra, G., Seton, M., & Giardini, D. (2011). Signatures
710 of downgoing plate-buoyancy driven subduction in Cenozoic plate motions.
711 *Physics of the Earth and Planetary Interiors*, *184*(1-2), 1–13.
- 712 Gutscher, M. A., Malavieille, J., Lallemand, S., & Collot, J. Y. (1999). Tectonic
713 segmentation of the North Andean margin: Impact of the Carnegie Ridge
714 collision. *Earth and Planetary Science Letters*, *168*(3-4), 255–270.
- 715 Gutscher, M. A., Olivet, J. L., Aslanian, D., Eissen, J. P., & Maury, R. (1999). The
716 “lost Inca Plateau”: Cause of flat subduction beneath Peru? *Earth and Plane-
717 tary Science Letters*, *171*(3), 335–341.
- 718 Hager, B. H., & Richards, A. M. (1989). Long-wavelength variations in Earth’s
719 geoid: Physical models and dynamical implications. *Phil. Trans. Roy. Soc.
720 London, Ser. A.*, *328*, 309–327.
- 721 Heuret, A., Funicello, F., Faccenna, C., & Lallemand, S. (2007). Plate kinematics,
722 slab shape and back-arc stress: A comparison between laboratory models and
723 current subduction zones. *Earth and Planetary Science Letters*, *256*(3-4),
724 473–483.
- 725 Heuret, A., Lallemand, S., Funicello, F., Piromallo, C., & Faccenna, C. (2011).
726 Physical characteristics of subduction interface type seismogenic zones revis-
727 ited. *Geochemistry, Geophysics, Geosystems*, *12*(1).
- 728 Holt, A. F., & Royden, L. H. (2020). Subduction dynamics and mantle pressure: 2.
729 towards a global understanding of slab dip and upper mantle circulation. *Geo-
730 chemistry, Geophysics, Geosystems*, *21*(7), e2019GC008771.
- 731 Holt, A. F., Royden, L. H., & Becker, T. W. (2017). The dynamics of double slab
732 subduction. *Geophysical Journal International*, *209*(1), 250–265.

- 733 Holt, A. F., Royden, L. H., Becker, T. W., & Faccenna, C. (2018). Slab interactions
734 in 3-d subduction settings: The philippine sea plate region. *Earth and Plane-*
735 *tary Science Letters*, *489*, 72–83.
- 736 Jarrard, R. D. (1986). Relations among subduction parameters. *Reviews of Geo-*
737 *physics*, *24*(2), 217–284.
- 738 Karato, S.-i., Riedel, M. R., & Yuen, D. A. (2001). Rheological structure and de-
739 formation of subducted slabs in the mantle transition zone: Implications for
740 mantle circulation and deep earthquakes. *Physics of the Earth and Planetary*
741 *Interiors*, *127*(1-4), 83–108.
- 742 Kearey, P., Klepeis, K. A., & Vine, F. J. (2009). *Global tectonics*. John Wiley &
743 Sons.
- 744 Kimura, G., Kitamura, Y., Yamaguchi, A., Kameda, J., Hashimoto, Y., & Hama-
745 hashi, M. (2019). Origin of the early cenozoic belt boundary thrust and
746 izanagi–pacific ridge subduction in the western pacific margin. *Island Arc*,
747 *28*(5), e12320.
- 748 Kramer, S. C., Davies, D. R., & Wilson, C. R. (2021). Analytical solutions for man-
749 tle flow in cylindrical and spherical shells. *Geoscientific Model Development*,
750 *14*(4), 1899–1919.
- 751 Kramer, S. C., Wilson, C. R., & Davies, D. R. (2012). An implicit free surface algo-
752 rithm for geodynamical simulations. *Physics of the Earth and Planetary Interi-*
753 *ors*, *194*, 25–37.
- 754 Lallemand, S., Heuret, A., & Boutelier, D. (2005). On the relationships between
755 slab dip, back-arc stress, upper plate absolute motion, and crustal nature in
756 subduction zones. *Geochemistry, Geophysics, Geosystems*, *6*(9).
- 757 Laravie, J. A. (1975). Geometry and lateral strain of subducted plates in island arcs.
758 *Geology*, *3*(9), 484–486.
- 759 Le Voci, G., Davies, D. R., Goes, S., Kramer, S. C., & Wilson, C. R. (2014).
760 A systematic 2-D investigation into the mantle wedge’s transient flow
761 regime and thermal structure: complexities arising from a hydrated rheol-
762 ogy and thermal buoyancy. *Geochem. Geophys. Geosys.*, *15*, 28–51. doi:
763 10.1002/2013GC005022
- 764 Li, C., van der Hilst, R. D., Engdahl, E. R., & Burdick, S. (2008). A new global
765 model for P wave speed variations in Earth’s mantle. *Geochemistry, Geo-*
766 *physics, Geosystems*, *9*(5).
- 767 Lithgow-Bertelloni, C., & Richards, M. A. (1998). The dynamics of Cenozoic and
768 Mesozoic plate motions. *Reviews of Geophysics*, *36*(1), 27–78.
- 769 Lonsdale, P. (2005). Creation of the Cocos and Nazca plates by fission of the Faral-
770 lon plate. *Tectonophysics*, *404*(3-4), 237–264.
- 771 Mahadevan, L., Bendick, R., & Liang, H. (2010). Why subduction zones are curved.
772 *Tectonics*, *29*(6).
- 773 Mann, P., & Taira, A. (2004). Global tectonic significance of the Solomon Islands
774 and Ontong Java Plateau convergent zone. *Tectonophysics*, *389*(3-4), 137–190.
- 775 Martinod, J., Funicello, F., Faccenna, C., Labanieh, S., & Regard, V. (2005). Dy-
776 namical effects of subducting ridges: insights from 3-D laboratory models.
777 *Geophysical Journal International*, *163*(3), 1137–1150.
- 778 Martinod, J., Husson, L., Roperch, P., Guillaume, B., & Espurt, N. (2010). Horizontal
779 subduction zones, convergence velocity and the building of the andes. *Earth*
780 *and Planetary Science Letters*, *299*(3-4), 299–309.
- 781 Mason, W. G., Moresi, L., Betts, P. G., & Miller, M. S. (2010). Three-dimensional
782 numerical models of the influence of a buoyant oceanic plateau on subduction
783 zones. *Tectonophysics*, *483*(1-2), 71–79.
- 784 McKenzie, D., Jackson, J., & Priestley, K. (2005). Thermal structure of oceanic and
785 continental lithosphere. *Earth and Planetary Science Letters*, *233*(3-4), 337–
786 349.
- 787 Mitrovica, J. X., Beaumont, C., & Jarvis, G. T. (1989). Tilting of continental inte-

- 788 riors by the dynamical effects of subduction. *Tectonics*, 8, 1079-1094. doi: 10
789 .1029/TC008i005p01079
- 790 Morra, G., Chatelain, P., Tackley, P., & Koumoutsakos, P. (2009). Earth curvature
791 effects on subduction morphology: Modeling subduction in a spherical setting.
792 *Acta Geotechnica*, 4(2), 95–105.
- 793 Morra, G., Quevedo, L., & Müller, R. D. (2012). Spherical dynamic models of top-
794 down tectonics. *Geochemistry, Geophysics, Geosystems*, 13(3).
- 795 Morra, G., Regenauer-Lieb, K., & Giardini, D. (2006). Curvature of oceanic arcs.
796 *Geology*, 34(10), 877–880.
- 797 Müller, R. D., Seton, M., Zahirovic, S., Williams, S. E., Matthews, K. J., Wright,
798 N. M., . . . Cannon, J. (2016). Ocean basin evolution and global-scale plate
799 reorganization events since Pangea breakup. *Annual Review of Earth and*
800 *Planetary Sciences*, 44, 107–138.
- 801 Müller, R. D., Zahirovic, S., Williams, S. E., Cannon, J., Seton, M., Bower, D. J., . . .
802 Gurnis, M. (2019). A global plate model including lithospheric deformation
803 along major rifts and orogens since the Triassic. *Tectonics*, 38(6), 1884–1907.
- 804 Neal, C. R., Mahoney, J. J., Kroenke, L. W., Duncan, R. A., & Petterson, M. G.
805 (1997). The Ontong Java Plateau. *Geophysical Monograph-American Geophys-*
806 *ical Union*, 100, 183–216.
- 807 OzBench, M., Regenauer-Lieb, K., Stegman, D. R., Morra, G., Farrington, R., Hale,
808 A., . . . Moresi, L. (2008). A model comparison study of large-scale mantle–
809 lithosphere dynamics driven by subduction. *Physics of the Earth and Plane-*
810 *tary Interiors*, 171(1-4), 224–234.
- 811 Pelletier, B., Calmant, S., & Pillet, R. (1998). Current tectonics of the Tonga–New
812 Hebrides region. *Earth and Planetary Science Letters*, 164(1-2), 263–276.
- 813 Perrin, A., Goes, S., Prytulak, J., Rondenay, S., & Davies, D. R. (2018). Mantle
814 wedge temperatures and their potential relation to volcanic arc location. *Earth*
815 *and Planetary Science Letters*, 501, 67–77.
- 816 Ribe, N. M. (2010). Bending mechanics and mode selection in free subduction: A
817 thin-sheet analysis. *Geophysical Journal International*, 180(2), 559–576.
- 818 Rodríguez-González, J., Negredo, A. M., & Billen, M. I. (2012). The role of the
819 overriding plate thermal state on slab dip variability and on the occurrence of
820 flat subduction. *Geochemistry, Geophysics, Geosystems*, 13(1).
- 821 Rubey, M., Brune, S., Heine, C., Davies, D. R., Williams, S. E., & Müller, R. D.
822 (2017). Global patterns in Earth’s dynamic topography since the Jurassic: the
823 role of subducted slabs. *Solid Earth*, 8, 899-919. doi: 10.5194/se-8-899-2017
- 824 Schellart, W. P. (2004). Kinematics of subduction and subduction-induced flow in
825 the upper mantle. *Journal of Geophysical Research: Solid Earth*, 109(B7).
- 826 Schellart, W. P. (2008). Kinematics and flow patterns in deep mantle and upper
827 mantle subduction models: Influence of the mantle depth and slab to mantle
828 viscosity ratio. *Geochemistry, Geophysics, Geosystems*, 9(3).
- 829 Schellart, W. P., Freeman, J., Stegman, D. R., Moresi, L., & May, D. (2007). Evo-
830 lution and diversity of subduction zones controlled by slab width. *Nature*,
831 446(7133), 308–311.
- 832 Schepers, G., van Hinsbergen, D. J., Spakman, W., Kosters, M. E., Boschman,
833 L. M., & McQuarrie, N. (2017). South-American plate advance and forced
834 Andean trench retreat as drivers for transient flat subduction episodes. *Nature*
835 *communications*, 8(1), 1–9.
- 836 Schettino, A., & Tassi, L. (2012). Trench curvature and deformation of the subduct-
837 ing lithosphere. *Geophysical Journal International*, 188(1), 18–34.
- 838 Scholl, D. W., Buffington, E. C., & Marlow, M. S. (1975). Plate tectonics and the
839 structural evolution of the Aleutian–Bering Sea region. *Geological Society of*
840 *America Special Papers*, 151, 1–32.
- 841 Sdrolias, M., & Müller, R. D. (2006). Controls on back-arc basin formation. *Geo-*
842 *chemistry, Geophysics, Geosystems*, 7(4).

- 843 Sharples, W., Jadamec, M. A., Moresi, L.-N., & Capitanio, F. A. (2014). Overriding
844 plate controls on subduction evolution. *Journal of Geophysical Research: Solid*
845 *Earth*, *119*(8), 6684–6704.
- 846 Stegman, D. R., Farrington, R., Capitanio, F. A., & Schellart, W. P. (2010). A
847 regime diagram for subduction styles from 3-D numerical models of free sub-
848 duction. *Tectonophysics*, *483*(1-2), 29–45.
- 849 Stegman, D. R., Freeman, J., Schellart, W. P., Moresi, L., & May, D. (2006). Influ-
850 ence of trench width on subduction hinge retreat rates in 3-D models of slab
851 rollback. *Geochemistry, Geophysics, Geosystems*, *7*(3).
- 852 Stegman, D. R., Schellart, W. P., & Freeman, J. (2010). Competing influences of
853 plate width and far-field boundary conditions on trench migration and mor-
854 phology of subducted slabs in the upper mantle. *Tectonophysics*, *483*(1-2),
855 46–57.
- 856 Stern, R. J. (2002). Subduction zones. *Reviews of geophysics*, *40*(4), 3–1.
- 857 Stotz, I. L., Iaffaldano, G., & Davies, D. R. (2017). Late Miocene Pacific plate kine-
858 matic change explained with coupled global models of mantle and lithosphere
859 dynamics. *Geophysical Research Letters*, *44*(14), 7177–7186.
- 860 Strak, V., & Schellart, W. P. (2016). Control of slab width on subduction-induced
861 upper mantle flow and associated upwellings: Insights from analog models.
862 *Journal of Geophysical Research: Solid Earth*, *121*(6), 4641–4654.
- 863 Suchoy, L., Goes, S., Chen, F., & Davies, R. (2022). How aseismic ridges modify the
864 dynamics of free subduction: a 3-d numerical investigation. *Frontiers in Earth*
865 *Science*, 611.
- 866 Suchoy, L., Goes, S., Maunder, B., Garel, F., & Davies, R. (2021). Effects of basal
867 drag on subduction dynamics from 2d numerical models. *Solid Earth*, *12*(1),
868 79–93.
- 869 Tanimoto, T. (1998). State of stress within a bending spherical shell and its impli-
870 cations for subducting lithosphere. *Geophysical Journal International*, *134*(1),
871 199–206.
- 872 Torii, Y., & Yoshioka, S. (2007). Physical conditions producing slab stagnation:
873 Constraints of the Clapeyron slope, mantle viscosity, trench retreat, and dip
874 angles. *Tectonophysics*, *445*(3-4), 200–209.
- 875 Tosi, N., Stein, C., Noack, L., Hüttig, C., Maierová, P., Samuel, H., . . . Tackley,
876 P. J. (2015). A community benchmark for viscoplastic thermal convection in a
877 2-d square box. *Geochemistry, Geophysics, Geosystems*, *16*(7), 2175–2196. doi:
878 10.1002/2015GC005807
- 879 van der Hilst, R., & Seno, T. (1993). Effects of relative plate motion on the deep
880 structure and penetration depth of slabs below the Izu-Bonin and Mariana
881 island arcs. *Earth and Planetary Science Letters*, *120*(3-4), 395–407.
- 882 van der Meer, D. G., van Hinsbergen, D. J., & Spakman, W. (2018). Atlas of the
883 underworld: Slab remnants in the mantle, their sinking history, and a new
884 outlook on lower mantle viscosity. *Tectonophysics*, *723*, 309–448.
- 885 van Dinther, Y., Morra, G., Funicello, F., & Faccenna, C. (2010). Role of the
886 overriding plate in the subduction process: Insights from numerical models.
887 *Tectonophysics*, *484*(1-4), 74–86.
- 888 van Hunen, J., van den Berg, A. P., & Vlaar, N. J. (2002). On the role of subduct-
889 ing oceanic plateaus in the development of shallow flat subduction. *Tectono-*
890 *physics*, *352*(3-4), 317–333.
- 891 Wheeler, P., & White, N. (2002). Measuring dynamic topography: An analysis of
892 Southeast Asia. *Tectonics*, *21*(5), 4–1.
- 893 Whittaker, J. M., Müller, R. D., Sdrolias, M., & Heine, C. (2007). Sunda-Java
894 trench kinematics, slab window formation and overriding plate deformation
895 since the Cretaceous. *Earth and Planetary Science Letters*, *255*(3-4), 445–457.
- 896 Wilson, C. R. (2009). *Modelling multiple-material flows on adaptive unstructured*
897 *meshes*. PhD Thesis, Imperial College London, UK.

898 Yamaoka, K. (1988). Spherical shell tectonics: on the buckling of the lithosphere at
899 subduction zones. *Tectonophysics*, 147(3-4), 179–191.